



**HAL**  
open science

## **Fate of trace organic compounds in the hyporheic zone: influence of retardation, the benthic bio-layer and organic carbon**

Jonas Schaper, Malte Posselt, Camille Bouchez, Anna Jaeger, Gunnar Nuetzmann, Anke Putschew, Gabriel Singer, Jörg Lewandowski

### ► To cite this version:

Jonas Schaper, Malte Posselt, Camille Bouchez, Anna Jaeger, Gunnar Nuetzmann, et al.. Fate of trace organic compounds in the hyporheic zone: influence of retardation, the benthic bio-layer and organic carbon. *Environmental Science and Technology*, 2019, 53 (8), pp.4224-4234. 10.1021/acs.est.8b06231 . insu-02082924

**HAL Id: insu-02082924**

**<https://insu.hal.science/insu-02082924>**

Submitted on 28 Mar 2019

**HAL** is a multi-disciplinary open access archive for the deposit and dissemination of scientific research documents, whether they are published or not. The documents may come from teaching and research institutions in France or abroad, or from public or private research centers.

L'archive ouverte pluridisciplinaire **HAL**, est destinée au dépôt et à la diffusion de documents scientifiques de niveau recherche, publiés ou non, émanant des établissements d'enseignement et de recherche français ou étrangers, des laboratoires publics ou privés.

## Fate of trace organic compounds in the hyporheic zone: influence of retardation, the benthic bio-layer and organic carbon

Jonas Schaper, Malte Posselt, Camille Bouchez, Anna Jaeger, Gunnar Nützmann, Anke Putschew, Gabriel Singer, and Jörg Lewandowski

*Environ. Sci. Technol.*, **Just Accepted Manuscript** • Publication Date (Web): 24 Mar 2019

Downloaded from <http://pubs.acs.org> on March 28, 2019

### Just Accepted

“Just Accepted” manuscripts have been peer-reviewed and accepted for publication. They are posted online prior to technical editing, formatting for publication and author proofing. The American Chemical Society provides “Just Accepted” as a service to the research community to expedite the dissemination of scientific material as soon as possible after acceptance. “Just Accepted” manuscripts appear in full in PDF format accompanied by an HTML abstract. “Just Accepted” manuscripts have been fully peer reviewed, but should not be considered the official version of record. They are citable by the Digital Object Identifier (DOI®). “Just Accepted” is an optional service offered to authors. Therefore, the “Just Accepted” Web site may not include all articles that will be published in the journal. After a manuscript is technically edited and formatted, it will be removed from the “Just Accepted” Web site and published as an ASAP article. Note that technical editing may introduce minor changes to the manuscript text and/or graphics which could affect content, and all legal disclaimers and ethical guidelines that apply to the journal pertain. ACS cannot be held responsible for errors or consequences arising from the use of information contained in these “Just Accepted” manuscripts.

1 Fate of trace organic compounds in the hyporheic zone: influence of  
2 retardation, the benthic bio-layer and organic carbon

---

3 JONAS L. SCHAPER<sup>1,2\*</sup>, MALTE POSSELT,<sup>3</sup> CAMILLE BOUCHEZ,<sup>4</sup> ANNA JAEGER,<sup>1,5</sup> GUNNAR  
4 NUETZMANN,<sup>1,5</sup> ANKE PUTSCHEW,<sup>2</sup> GABRIEL SINGER,<sup>1</sup> AND JOERG LEWANDOWSKI<sup>1,5</sup>

5 <sup>1</sup> Leibniz-Institute of Freshwater Ecology and Inland Fisheries, Department Ecohydrology, Müggelseedamm 310,  
6 12587 Berlin, Germany

7 <sup>2</sup> Technische Universität Berlin, Chair of Water Quality Engineering, Strasse des 17. Juni 135, 10623 Berlin,  
8 Germany

9 <sup>3</sup> Department of Environmental Science and Analytical Chemistry (ACES), Stockholm University, Stockholm,  
10 Sweden

11 <sup>4</sup> Univ Rennes, CNRS, Géosciences Rennes, UMR 6118, 35000 Rennes, France

12 <sup>5</sup> Humboldt University Berlin, Geography Department, Rudower Chaussee 16, 12489 Berlin, Germany

13

14

15 \*corresponding author; [schaper@igb-berlin.de](mailto:schaper@igb-berlin.de), Leibniz-Institute of Freshwater Ecology and Inland Fisheries,  
16 Department Ecohydrology, Müggelseedamm 310, 12587 Berlin, Germany

17

**18 Abstract**

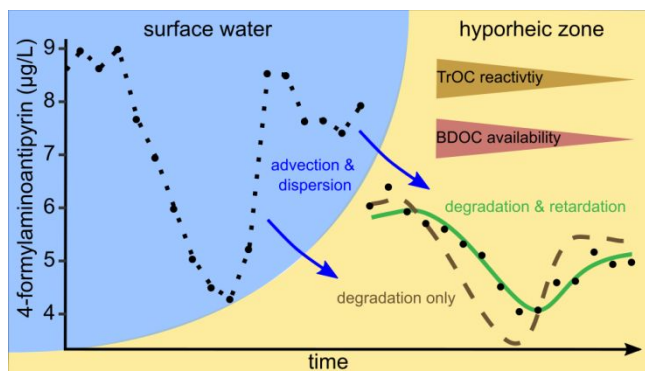
19 The fate of 28 trace organic compounds (TrOCs) was investigated in the hyporheic zone (HZ) of an urban  
20 lowland river in Berlin, Germany. Water samples were collected hourly over 17 h in the river and in three  
21 depths in the HZ using minipoint samplers. The four relatively variable time series were subsequently  
22 used to calculate first-order removal rates and retardation coefficients via a one-dimensional reactive  
23 transport model. Reversible sorption processes led to substantial retardation of many TrOCs along the  
24 investigated hyporheic flow path. Some TrOCs such as dihydroxy-carbamazepine, O-  
25 desmethylvenlafaxine and venlafaxine were found to be stable in the HZ. Others were readily removed  
26 with half-lives in the first 10 cm of the HZ ranging from  $0.1 \pm 0.01$  h for iopromide to  $3.3 \pm 0.3$  h for  
27 tramadol. Removal rate constants of the majority of reactive TrOCs were highest in the first 10 cm of the  
28 HZ, where removal of biodegradable dissolved organic matter was also highest. Because conditions were  
29 oxic along the top 30 cm of the investigated flow path we attribute this finding to the high microbial  
30 activity typically associated with the shallow HZ. Frequent and short vertical hyporheic exchange flows  
31 could therefore be more important for reach-scale TrOC removal than long, lateral hyporheic flow paths.

32 **Keywords**

33 Pharmaceuticals, metformin, guanylurea, urban water cycle, reactive transport modeling

34 **TOC Art**

35



## 36 **Introduction**

37 Many trace organic compounds such as pharmaceuticals are only partially retained in wastewater  
38 treatment plants (WWTPs)<sup>1,2</sup> and thus are ubiquitous in urban surface waters.<sup>3,4</sup> In rivers, TrOCs are of  
39 eco-toxicological concern<sup>5-7</sup> and the high persistence of some TrOCs in aquatic environments poses issues  
40 for drinking water production.<sup>8</sup> The hyporheic zone (HZ), the portion of the streambed in which surface  
41 waters and groundwater mix,<sup>9</sup> is generally regarded as an effective bioreactor, characterized by steep  
42 redox gradients, diverse microbial communities and relatively high microbial turnover rates.<sup>10,11</sup> Both  
43 laboratory<sup>12,13</sup> and field studies<sup>14,15</sup> demonstrated that the HZ is able to efficiently remove many TrOCs,  
44 even along relatively short flow paths (< 20 cm). Therefore, the HZ may not only act as a filter protecting  
45 groundwater from surface water contamination<sup>16</sup> but also contributes to whole-stream, i.e. reach-scale  
46 attenuation of TrOCs.<sup>17</sup>

47 The adequate assessment of the in-situ efficiency of the HZ in removing TrOCs requires a sound  
48 understanding of both the in-situ reactivity and the exposure time of TrOCs to favorable attenuation  
49 conditions. Hyporheic residence times are predominately controlled by transport characteristics such as  
50 porewater velocity and dispersion. However, residence times of TrOCs along hyporheic flow paths may  
51 also be influenced by sorption and desorption processes, i.e. retardation.<sup>18-20</sup> Retardation can extend  
52 residence times of TrOCs in the HZ and, if not considered in reactive transport modeling, may lead to an  
53 overestimation of the in-situ reactivity of TrOCs in the HZ. Although retardation of some TrOCs in  
54 saturated sediments has been demonstrated in laboratory studies<sup>20,21</sup> little is known about its driving  
55 factors and its overall importance for transport of TrOCs in hyporheic sediments.

56 Reactivity of TrOCs in the HZ increases with temperature<sup>12</sup> and, for many TrOCs, is higher under oxic  
57 conditions.<sup>12,14</sup> However, since microbially mediated degradation and transformation mechanisms are  
58 considered to be a main driver of TrOC removal in saturated sediments, it is likely that TrOC reactivity in  
59 the HZ is also linked to microbial activity and growth and therefore to turnover of biodegradable dissolved  
60 organic matter (BDOC).<sup>22</sup> It has been shown that microbial activity in the HZ is typically highest in the

61 shallow HZ (within the so called benthic bio-layer), where BDOC availability is highest and redox  
62 conditions are rather oxidic.<sup>10,23,24</sup> It is therefore reasonable to assume that removal rates of TrOCs may vary  
63 substantially along hyporheic flow paths, even if redox conditions are relatively similar. In previous  
64 investigations on the fate of TrOCs in the HZ, neither retardation nor the effect of benthic bio-layers and  
65 depth-dependent transport characteristics on the fate of TrOCs has been considered.<sup>14,15,25</sup> In addition,  
66 previous studies have mainly investigated the fate of parent TrOCs in the HZ,<sup>14,15,25</sup> while information on  
67 the fate of transformation products (TPs) such as guanidylurea, the main TP of the antidiabetic drug  
68 metformin, valsartan acid, the main TP of compounds of the sartan group, or gabapentin-lactam a main TP  
69 of the anticonvulsant gabapentin in the HZ is widely lacking.

70 The objectives of the present study were to use concentration time series of TrOCs and conservative  
71 tracers sampled along a 40 cm long hyporheic flow path to calculate depth-dependent in-situ retardation  
72 coefficients and first-order removal rate constants of 28 TrOCs, including 7 transformation products, in  
73 the HZ of an urban lowland river in Berlin, Germany. We hypothesize that hyporheic reactivities of  
74 TrOCs are highest in the shallow HZ, where redox conditions are rather oxidic and microbial activity is  
75 highest. We further anticipate that many TrOCs are retarded along hyporheic flow paths, which notably  
76 influences their residence times in the HZ and thus the estimation of hyporheic removal rates.

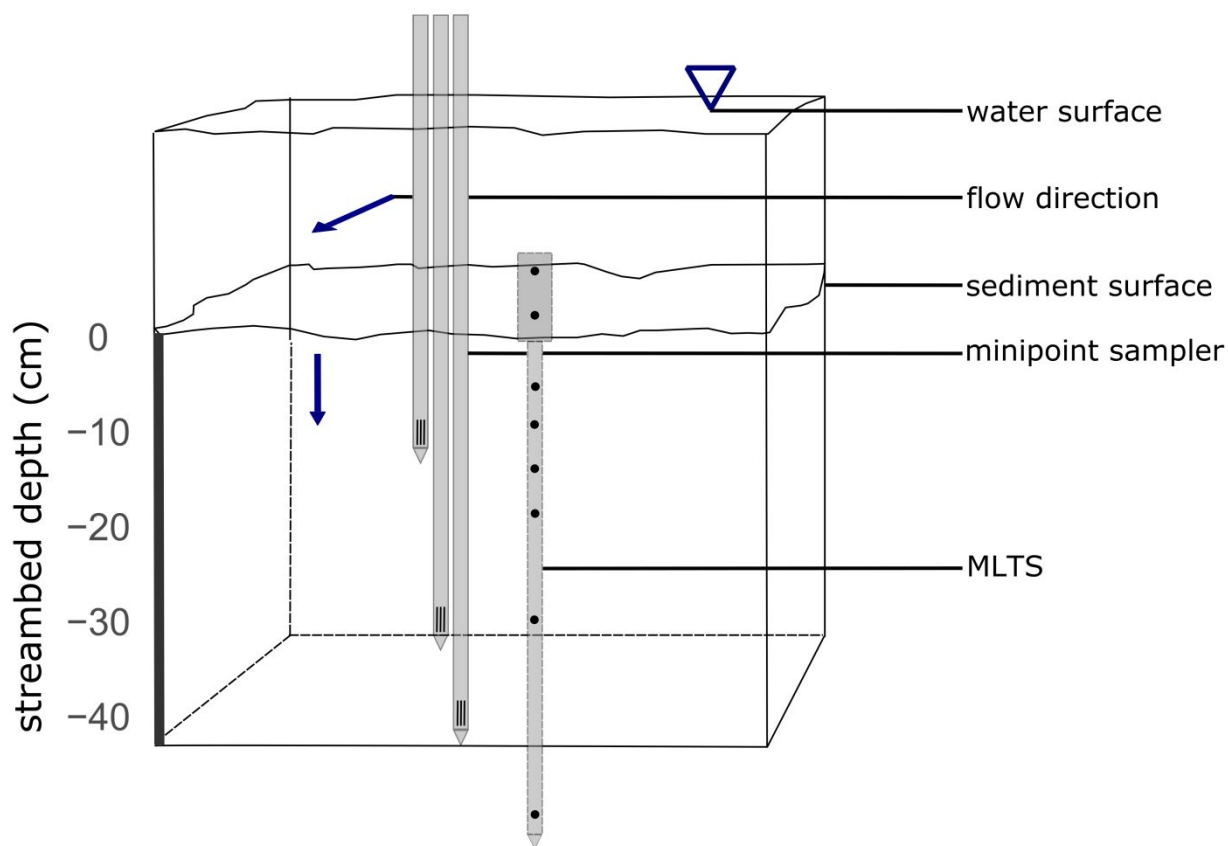
## 77 2. Methods

### 78 2.1 Site description and experimental overview

79 River Erpe, an urban lowland river located east of Berlin, Germany, receives 60% to 80% of its discharge  
80 from the municipal WWTP Münchehofe. The present study was conducted at Heidemühle (Lat:  
81 52.478647, Long: 13.635146), a section of River Erpe that has been subject to previous investigations on  
82 the fate of TrOCs in the HZ due to its sandy streambed sediments.<sup>14,15,26</sup> Sediment characteristics at the  
83 sampling site were determined from one 40 cm long sediment core which was taken using a hand auger  
84 (inner diameter 9 cm) in close proximity of the sampling site (< 10 cm) and cut into 8 cm long sections,  
85 which were transferred into 5 KSAT rings (Meter, Germany) on site. Saturated hydraulic conductivity at  
86 25 °C was measured using a KSAT device (Meter, Germany) and ranged between  $1.6 \times 10^{-5} \text{ m s}^{-1}$  and  $1.7$   
87  $\times 10^{-4} \text{ m s}^{-1}$ . Porosity, determined from oven dried (105 °C, 48h) samples, decreased from 0.5 in the upper  
88 8 cm of the HZ to 0.4 in the last 2 sub-cores (i.e. 24-40 cm depth).

89 The experimental setup consisted of three self-constructed mini-point samplers<sup>26</sup> (compare section 2.2)  
90 that were installed in the HZ in 10, 30 and 40 cm depth (Figure 1). An additional mini-point sampler was  
91 installed in the HZ in 20 cm depth. However, due to clogging, the sampler in 20 cm depth provided only a  
92 limited number of samples and was thus excluded from further analysis. To gain additional information on  
93 the hydrological conditions at the study site and to cross-check porewater velocities determined by  
94 conservative transport modeling (section 2.5), porewater velocities were additionally calculated from  
95 temperature time series in the HZ. To this end, a Multi-Level Temperature Stick<sup>27</sup> (MLTS, UIT, Dresden)  
96 was installed adjacent to the minipoint samplers ( $\approx 10 \text{ cm}$ ). Temperature time series were collected over  
97 the course of two weeks (14.06.-28.06.2016) in 5, 10, 15, 20, 30 and 50 cm depth in the HZ.  
98 Subsequently, vertical seepage fluxes and thermal dispersion coefficients were evaluated via the  
99 McCallum method<sup>28</sup> incorporated in the VFLUX 2.0 program.<sup>29</sup> The McCallum method simultaneously  
100 uses phase shifts ( $\Delta\phi$ ) and amplitude damping ratios ( $A_r$ ) of two sinusoidal temperature time series to  
101 calculate both the thermal dispersivity and the Darcy velocity via an analytical solution of the one-

102 dimensional heat transport equation. In VFLUX, dynamic harmonic regression,<sup>30</sup> a form of harmonic  
 103 regression in which the spectral coefficients describing a periodic signal can be non-stationary, is used to  
 104 estimate phase and amplitude information from the measured time series. Vertical seepage fluxes and  
 105 thermal dispersion coefficients were calculated from measured temperature time series in 5 and 10 cm, 10  
 106 and 30 cm and 20 and 50 cm depth in the HZ, yielding parameter estimates at center-of-pair depths of 7.5  
 107 cm, 20 cm and 35 cm, respectively, covering the three different model sections in the HZ (compare  
 108 section 2.5). Further details on the method and its underlying assumptions can be found elsewhere<sup>14,26</sup> and  
 109 in the Supporting Information (SI, section SI-01).



110  
 111 **Figure 1** Experimental setup showing the three minipoint sampler installed in 10 cm, 30 cm and 40 cm depth in the hyporheic  
 112 zone (HZ). The samplers were installed in a line (< 1 cm distance) perpendicular to the water flow direction. A Multilevel  
 113 Temperature Stick (MLTS) was installed in close proximity ( $\approx 10$  cm) next to the minipoint sampler array. Blue arrows indicate  
 114 surface water and predominant hyporheic flow directions. Minipoint samplers were sampled from an aluminum bridge spanning  
 115 the river channel (not shown).

116

## 117 **2.2 Water sampling**

118 Hyporheic porewater samples were collected hourly between 22:30 on June, 15<sup>th</sup> and 15:30 on June 16<sup>th</sup>  
119 2016 using self-constructed mini-point samplers.<sup>26</sup> In brief, the mini-points consisted of HPLC tubes  
120 (PEEK, ID 0.03 inch, Sigma Aldrich, USA) that were inserted into 1.5 m long stainless steel tubes (ID 0.7  
121 mm). At the tip of the steel tubes, four 1-cm long laser cut slits (< 0.1 mm) allowed water flow but acted  
122 as a filter screen for most sediment particles. The HPLC tubes were connected to a syringe pump (NE-  
123 1600 New Era Pump Systems, Inc, Farmingdale, USA) via Swagelok fittings (Swagelok, USA) to allow  
124 slow, constant pumping of hyporheic porewater. Thirteen ml of hyporheic porewater were sampled  
125 applying a constant sampling rate of 1 ml min<sup>-1</sup>. In previous investigations conducted at the same site  
126 pumping rates of 1 ml min<sup>-1</sup> have been found to be sufficiently low to maintain the integrity of the  
127 hyporheic flow field.<sup>26</sup> Electrical conductivity (EC) was measured in each sample and in the surface water  
128 using handheld EC meters (GMH 3431, Greisinger, Germany). Every four hours, pH was measured in the  
129 hyporheic porewater samples and in the surface water using a handheld pH meter (SenTix 41, WTW,  
130 Germany), calibrated prior to sampling. Samples in the HZ were related to surface water samples,  
131 obtained from an automatic water sampler (model 3700, Teflon suction line, Teledyne ISCO, Lincoln,  
132 NE.) located 150 m upstream of the sampling site following procedures described elsewhere.<sup>31</sup> Samples  
133 for TrOC and dissolved organic carbon (DOC) analysis were filtered through regenerated cellulose  
134 syringe filters (0.2 μm, Macherey-Nagel, Germany) and stored in amber glass bottles with Teflon lined  
135 caps. Samples for TrOC analysis were immediately frozen on site. Samples for DOC analysis were stored  
136 at 4° C in the dark and were measured within two weeks after sampling. Samples for NO<sub>3</sub><sup>-</sup>-N and major  
137 cation analysis were filtered through cellulose acetate syringe filters (0.2 μm, Sartorius, Germany) and  
138 stored in polyethylene bottles at 4 °C until analysis. Samples for total dissolved iron and dissolved  
139 manganese analysis were additionally acidified to pH ≈ 2.0 using HCl. A sampling period of 17 h was  
140 considered sufficient as the aim of the present study was to investigate TrOC reactivity and the effect of  
141 retardation on TrOC transport along a relatively constrained hyporheic flow path. From previous studies at

142 the same field site it was known that (i) chemical conditions in River Erpe oscillate on a daily basis  
143 (concentration troughs in the morning, peaks in the afternoon) but are relatively constant over the course  
144 of weeks and (ii) that porewater velocities were in the order of several cm per hour.<sup>14,31</sup>

145

### 146 **2.3 Analytical procedures**

147 To enlarge the number of target compounds, samples were split and analyzed in parallel using high  
148 performance liquid chromatography with tandem mass spectrometry (HPLC-MS/MS) at the Department  
149 of Environmental Science and Analytical Chemistry (ACES) at Stockholm University and the Chair of  
150 Water Quality Engineering at Technical University of Berlin (TUB) following standard protocols  
151 established previously.<sup>26,32,33</sup> In brief, separation of TrOCs was achieved via a XSelect HSS T3 HPLC  
152 column (2.5  $\mu\text{m}$  particle size, 2.1 \* 50 mm, Waters, USA) at TUB and an Acquity UPLC HSS T3 column  
153 (1.8  $\mu\text{m}$ , 2.1 mm  $\times$  100 mm, Waters, USA) at ACES. Both protocols used linear gradients (ultra-pure  
154 water versus 100% methanol; HPLC grade, J.T. Baker, USA). A TSQ Vantage (Thermo Fisher Scientific,  
155 USA) and a Quantiva triple-quadrupole mass spectrometer in ESI  $\pm$  modes were used for MS/MS analysis  
156 at TUB and ACES, respectively. In both methods, TrOC were identified based on the characteristic ratio  
157 of two ion fragments and quantified via isotope-substituted standards (Toronto Research Chemicals,  
158 Canada) in combination with the most abundant fragment ion (Table SI-01). In both methods, a series of  
159 calibration standards was measured before and after each sampling sequence. To assess analytical errors,  
160 samples at TUB were measured in triplicate, while at ACES quality control standards were measured  
161 during each run. In total, 29 TrOCs, including 22 parent compounds (PCs) and 7 transformation products  
162 (TPs), were analyzed in the present study. Ultra-pure water (Maxima UF device, ELGA LabWater,  
163 Germany) and tap water were measured as method blank at TUB and ACES, respectively. Limits of  
164 detection (LODs) and quantification (LOQs) for each target compound and additional information on the  
165 analytical procedures and data evaluation are provided in the SI (section 2). Concentrations of major  
166 cations and total dissolved iron and manganese were measured using inductively coupled plasma optical  
167 emission spectrometry (ICP-OES, ICP iCAP 6000series, Thermo Fisher). Nitrate-N concentrations were  
168 measured via continuous-flow-analysis (SAN ++, Skalar) following DIN EN ISO 13395.  
169 Absorbance spectra of dissolved organic matter (DOM, 250–600 nm, every 5 nm) and excitation-emission  
170 matrices (EEMs, excitation wavelength ranging from 250 to 600 nm, 5 nm increments; emission range of

171 250–550 nm 1.64 nm increments) were measured in triplicate at a Horiba Aqualog (Horiba Ltd, Japan) in  
 172 a 1 cm quartz cuvette. One blank (MiliQ water) was measured for every 9 measurements. Scan speed was  
 173 12 000 nm min<sup>-1</sup> at a response time of 0.01 s. The Humification Index (HIX), a measure of the degree of  
 174 humification of DOM,<sup>34</sup> was calculated after EEMs were blank-subtracted and corrected for the inner  
 175 filter effect. DOC concentration was measured in triplicate at a varioTOC cube (elementar  
 176 Analysensysteme, Germany). Specific UV absorbance at 254 nm (SUVA<sub>254</sub>) was calculated by  
 177 normalizing the decadal absorbance measured at 254 nm to DOC concentration (mg/L).<sup>35</sup>

## 178 2.4 Calculation of relative removal percentages

179 To assess overall TrOC removal along the investigated hyporheic flow path and to cross-validate  
 180 calculated removal rate constants (section 2.5), relative TrOC removals were calculated between the  
 181 surface water and hyporheic water in 40 cm depth and between other pairs of concentration time series,  
 182 i.e., between the surface water and hyporheic water in 10 cm depth, between hyporheic water in 10 and in  
 183 30 cm depth and between hyporheic water in 30 and in 40 cm depth. Because measured concentrations  
 184 varied with time, relative removal of a given TrOC (x) between two sampling depths (Rel<sub>x</sub>) was calculated  
 185 using cumulative concentrations of a TrOC normalized to cumulative concentrations of a stable reference  
 186 compound:<sup>36,37</sup>

$$\text{Rel}_x^{\text{in}-\text{out}} = \left( 1 - \frac{\sum_i^n c_{x,\text{out},i} \sum_i^n c_{\text{ref},\text{in},i}}{\sum_i^n c_{x,\text{in},i} \sum_i^n c_{\text{ref},\text{out},i}} \right) \times 100\% \quad (1)$$

187  
 188 whereby  $c_{x,\text{in}}$  and  $c_{x,\text{out}}$  ( $c_{\text{ref},\text{in}}$  and  $c_{\text{ref},\text{out}}$ ) are the concentrations of the upper and lower concentration time  
 189 series of a TrOC (a stable reference compound), respectively, and n is the number of data points in each  
 190 time series. In the present study we used *O*-desmethylvenlafaxine (MLX) as a stable reference compound  
 191 as it showed low retardation along the hyporheic flow path and was found to be rather stable in the HZ  
 192 (compare section 3.3). The approach was cross-validated using the diurnal varying EC signal measured in

193 the surface water and in hyporheic porewater samples as another conservative reference (SI section 4).  
194 Removal of a TrOC was considered significant if the 95% confidence interval of the relative removal,  
195 computed using the respective analytical uncertainties of each TrOC (Table SI-02), did not include zero.  
196 The applicability of equation 1 requires either relatively constant flow conditions or a positive correlation  
197 between the reference compound and the target TrOC concentrations. Both requirements were likely met  
198 in the present study as the study site was characterized by strong downwelling conditions (compare  
199 section 3.1) and concentrations of TrOCs (with the exception of acesulfame, metoprolol acid and  
200 metformin) were well correlated to *O*-desmethylvenlafaxine concentrations (Pearson Product Moment  
201 Correlation coefficients  $> 0.7$ ,  $p$ -value  $< 0.05$ ). Equation 1 is based on the assumption that the transport  
202 time scales of both, the target TrOC and the reference compound, are similar. Thus  $Rel_x$  calculated for  
203 strongly retarding TrOCs (compare section 3.4) should be treated with caution.  
204

## 205 **2.5 Reactive transport modeling**

206 Measured concentration time series in the HZ were evaluated using the one-dimensional (1D) advection-  
207 dispersion transport equation including first-order degradation and retardation (1D-ADE). Assuming  
208 steady and uniform flow in a homogeneous medium, and time invariant dispersion, retardation and first-  
209 order decay the 1D-ADE equation can be written as:

$$R\frac{\partial c}{\partial t} = D_h\frac{\partial^2 c}{\partial x^2} - v\frac{\partial c}{\partial x} - \lambda c \quad (2)$$

210 where  $c$  denotes the concentration of a (reactive) compound,  $D_h$  the effective hydrodynamic dispersion  
211 coefficient ( $\text{m}^2 \text{h}^{-1}$ ),  $v$  the vertical porewater velocity ( $\text{m h}^{-1}$ ),  $\lambda$  a first-order removal rate constant ( $\text{h}^{-1}$ ) and  
212  $R$  the retardation coefficient (-). Equation 2 was implemented in the programming language Python and  
213 solved numerically using a finite-difference scheme. The HZ was vertically divided into three sections  
214 delimited by each pair of concentration time series: Section 1 between the surface water and 10 cm depth,  
215 section 2 between 10 and 30 cm depth and section 3 between 30 and 40 cm depth. For each section in the  
216 HZ, equation 2 was solved separately, yielding independent parameter estimates for each section. The  
217 upper concentration time series served as an upper boundary condition in equation 2. The lower boundary  
218 condition (in 100, 110 and 120 cm depth for sections 1, 2 and 3, respectively) was set to zero. The lower  
219 concentration time series in each section was used for parameter estimation.

220 Parameter estimation was achieved using the DREAM algorithm,<sup>38,39</sup> a Bayesian parameter optimization  
221 method which employs evolutionary Monte Carlo Markov chains to estimate posterior probability density  
222 distributions (posteriors) of model parameters. In a first step, posteriors of conservative transport  
223 characteristics (i.e.  $v$  and  $D_h$ ) were estimated from EC time series by setting  $\lambda$  to zero and  $R$  to unity. In a  
224 second step, measured concentrations of TrOCs, DOC and  $\text{NO}_3^-$ -N were used to derive first-order removal  
225 rate constants and, for TrOCs, retardation coefficients using the previously derived posteriors for  $v$  and  $D_h$   
226 as priors. This approach was justified as the relative contribution of molecular diffusion to  $D_h$ , which at  
227 sediment-water interface is commonly described as the sum of molecular, hydrodynamic and turbulent

228 diffusivities,<sup>40,41</sup> can be considered negligible, because porewater velocities measured in the present study  
229 were larger than  $10^{-6}$  m s<sup>-1</sup> (compare section 3.1) and molecular diffusion coefficients ( $D_{mol}$ ) for the  
230 investigated TrOCs are generally smaller than  $10^{-9}$  m<sup>2</sup> s<sup>-1</sup> (Table SI-03, see SI section 3.3 for details on  
231 calculation of  $D_{mol}$ ).

232 Retardation coefficients can only be estimated from measured concentration time series that show a  
233 distinct, traceable temporal pattern, i.e., a trough or peak. For TrOCs, parameter optimization via DREAM  
234 was therefore conducted using two models, one including ( $R \geq 1$ ) and one excluding the effect of  
235 retardation ( $R=1$ ). If retardation coefficients could not be estimated, i.e., if posteriors of  $R$  were indifferent  
236 from their priors,  $\lambda$  was estimated from the model in which  $R$  was set to unity. The conceptual model of  
237 equation 2 assumes that i) water flows vertically from the surface into the HZ and that ii) mixing with  
238 groundwater can be neglected. These assumptions were justified as i) the study site was characterized by  
239 strong downwelling conditions (compare section 3.1) and a previous investigation on hyporheic flow  
240 fields at the same site found that horizontal flow components were of minor importance<sup>14</sup> and ii) relative  
241 removal of *O*-desmethylvenlafaxine, a stable reference compound (compare section 2.4), was calculated to  
242 be -3 to 4% (Table 2) indicating that groundwater input along the investigated flow path was negligible.  
243 Details on the numerical scheme used to solve equation 2 and the parameter estimation procedure  
244 including the prior distributions of model parameters and other DREAM settings are provided in the SI.

### 245 **3. Results & Discussion**

#### 246 **3.1 Transport characteristics in the hyporheic zone**

247 Median porewater velocities, estimated from temperature depth profiles using VFLUX, ranged between  
248 0.06 and 0.11 m h<sup>-1</sup> (Table 1). These strong downwelling conditions (positive flux = downward flow) are  
249 in line with values reported previously for the same study site.<sup>14</sup> As a result of low WWTP discharge  
250 during nighttime, EC time series in the surface water of River Erpe follow a saw-toothed pattern with  
251 distinct EC troughs in early morning hours.<sup>14</sup> The EC trough, measured in the surface water between 02:00

252 and 10:00 on June 16<sup>th</sup> propagated into the HZ and served as a natural tracer from which conservative  
 253 transport parameters were modeled using equation 2 (Figure 2). Porewater velocities derived from EC  
 254 time series using the 1D-ADE model ranged from 0.07 m h<sup>-1</sup> to 0.17 m h<sup>-1</sup> and are thus somewhat higher  
 255 than porewater velocities calculated from temperature time series using VFLUX, particularly in the upper  
 256 two sections of the HZ (Table 1). Differences in porewater velocities might be the result of erroneous  
 257 VFLUX calculations (e.g., due to violations of VFLUX model assumptions) and sediment heterogeneity.  
 258 Values for the effective hydrodynamic dispersion coefficient ( $D_h$ ) ranged between  $10 \times 10^{-4}$  and  $48 \times 10^{-4}$   
 259 m<sup>2</sup> h<sup>-1</sup> and are within the same order of magnitude as values of the effective thermal dispersion coefficient  
 260 calculated by VFLUX ( $D_t$ , Table 1).

261 **Table 1** Mean values ( $\pm 1$  standard deviation) of porewater velocities ( $v$ ) and dispersion coefficients (hydrodynamic dispersion  
 262 coefficient  $D_h$ , thermal dispersion coefficient  $D_t$ ) derived from i) electrical conductivity (EC) time series using eqn. 2 (1D-ADE)  
 263 and ii) from temperature time series using VFLUX 2.0 for all three sections in the hyporheic zone. In addition, removal rates of  
 264 NO<sub>3</sub><sup>-</sup>-N ( $k_{\text{nit-N}}$ ) and DOC ( $k_{\text{DOC}}$ ) are shown.

depth	1D-ADE		VFLUX 2.0		NO <sub>3</sub> <sup>-</sup> -N	DOC
	$v$	$D_h$	$v$	$D_t$	$k_{\text{nit-N}}$	$k_{\text{DOC}}$
cm	m h <sup>-1</sup>	m <sup>2</sup> h <sup>-1</sup> x 10 <sup>-4</sup>	m h <sup>-1</sup>	m <sup>2</sup> h <sup>-1</sup> x 10 <sup>-4</sup>	h <sup>-1</sup>	h <sup>-1</sup>
0-10	0.14 ± 0.01	48 ± 6	0.11 ± 0.02	73 ± 05	0.60 ± 0.03	0.30 ± 0.01
10-30	0.17 ± 0.01	10 ± 3	0.07 ± 0.01	34 ± 01	0.10 ± 0.01	0.12 ± 0.01
30-40	0.07 ± 0.01	46 ± 12	0.06 ± 0.01	36 ± 01	1.25 ± 0.03	0.05 ± 0.01

265

### 267 **3.2 Redox zonation and DOC dynamics in the hyporheic zone**

268 DOC concentrations gradually decreased along the investigated hyporheic flow path, while  $SUVA_{254}$  and  
269 HIX, measures of the aromaticity and the degree of humification of DOC, respectively increased (Figure  
270 SI-04). A general decrease of DOC concentrations and an increase of  $SUVA_{254}$  along hyporheic flow  
271 paths has been reported previously<sup>42</sup> and was attributed to preferred degradation of non-aromatic,  
272 biodegradable DOC fractions in the HZ. The largest removal rate of DOC as well as the largest change in  
273 HIX occurred between 0 and 10 cm depth (Table 1, Figure SI-04), suggesting that the largest change in  
274 DOC quantity and quality along the investigated hyporheic flow path occurred in the upper 10 cm of the  
275 HZ. This finding is in agreement with previous investigations in the HZ, suggesting that the highest  
276 carbon turnover rates in the HZ are typically found within the first cm of the HZ in the so called active  
277 benthic bio-layer.<sup>10</sup> A more detailed discussion of DOC dynamics in the HZ including information on  
278 other EEM indices is provided in the SI (SI section 6).

279 During the sampling period, nitrate concentrations in the surface water were high (median concentrations  
280 7.0 mg/L  $NO_3^-$ -N, Table SI-04). In the HZ, nitrate removal rates were high between 0 and 10 cm depth,  
281 low between 10 and 30 cm depth and highest between 30 and 40 cm depth (Figure SI-03, Table 1).  
282 Concentrations of total dissolved iron and dissolved manganese in the HZ were relatively low (< 0.05  
283 mg/L, Table SI-04), indicating the redox conditions in the stream sediment were not yet within iron- and  
284 manganese-reducing ranges. Removal of nitrate-N in the HZ can be caused by microbial uptake (i.e.,  
285 assimilation) and denitrification occurring in both anoxic sections of the HZ and in anoxic microzones.<sup>42-</sup>  
286 <sup>44</sup> Because DOC removal rates were highest in the shallow HZ, it is reasonable to assume that in addition  
287 to potential denitrification in anoxic microzones,<sup>23</sup> nitrate-N removal in the upper 10 cm in the HZ was  
288 primarily caused by biotic assimilation. The higher nitrate-N removal rate in the deeper HZ (i.e., between  
289 30 and 40 cm depth), however, is presumably attributable to denitrification. It is therefore likely that redox  
290 conditions in the bulk porewater were rather oxic in the first 30 cm of the HZ and became suboxic (i.e.  
291 denitrifying) thereafter. Redox zonation in the HZ is a function of biogeochemical parameters, such as

292 microbial turnover rates and the abundance and quality of electron acceptors and donors, physical  
293 parameters such as temperature and transport characteristics that control residence time distributions in the  
294 HZ. Compared to earlier investigations on redox zonation in the HZ at the same study site,<sup>14</sup> redox  
295 zonation in the present study was shifted downwards (i.e. deeper onset of denitrification and  
296 iron/manganese reduction). In line with previous studies,<sup>23</sup> we attribute this finding to larger porewater  
297 velocities measured in the present study.

298

### 299 **3.3 Reactivity of trace organic compounds in the HZ**

300 Out of the 29 investigated TrOCs, relative removals (%) and first-order removal rates could be calculated  
301 from measured concentration time series of 28 compounds (Table 2). For epoxy-carbamazepine (EBZ),  
302 concentrations were either below LOQ or just slightly above LOQ and thus EBZ was not considered in  
303 further analysis (Table SI-04). Modeled and measured concentration time series for valsartan acid (VSA),  
304 metformin (MEF) and its TP guanylurea (GUA) and EC are depicted in Figure 2. Measured and modeled  
305 concentration time series of the remaining TrOCs are shown in Figures SI 05-32. Twenty-two compounds  
306 were significantly removed between the surface water and 40 cm depth with half-lives within the first 10  
307 cm of the HZ ranging between  $0.1 \pm 0.01$  h for iopromide and  $3.5 \pm 0.3$  h for tramadol (Table 2).

308 The highest removal rate constants were calculated for the iodinated X-ray contrast agents iomeprol  
309 (IOM) and iopromide (IOP). Complete de-iodination of both compounds in saturated sediments has only  
310 been observed under anoxic redox conditions<sup>45</sup> but both compounds are known to readily lose side chains  
311 of the iodinated ring structure under aerobic conditions.<sup>46,47</sup> It is therefore likely that the high removal  
312 rates calculated in the present study are due to transformation of both compounds and do not represent  
313 complete mineralization. Removal of the artificial sweetener acesulfame (ACS), the lipid-lowering agent  
314 bezafibrate (BZF), the anti-corrosive agents benzotriazole and methylbenzotriazole and the anticonvulsant  
315 GAB along oxic to suboxic (i.e. denitrifying) flow paths in hyporheic sediments has previously been  
316 described in laboratory column experiments<sup>12,48</sup> and observed in the HZ.<sup>14</sup> For ACS, reported half-lives  
317 range from 1.2<sup>14</sup> to 5<sup>12</sup> h and for BZF and GAB were calculated to be 1.2 h and 0.96 h in a previous  
318 investigation at the same site.<sup>14</sup> Thus, half-lives for ACS, BZF and GAB calculated in the present study  
319 match half-lives calculated previously for hyporheic sediments. Removal of gabapentin-lactam, a major  
320 TP of GAB,<sup>48</sup> in saturated sediments has previously been reported during bank filtration, with half-lives  
321 between 1.2 and 3.7 h.<sup>49</sup> These values match the ones calculated for the first 10 cm of the HZ ( $2.3 \pm 0.2$  h),  
322 although no further removal of GPL was observed in deeper section of the HZ.

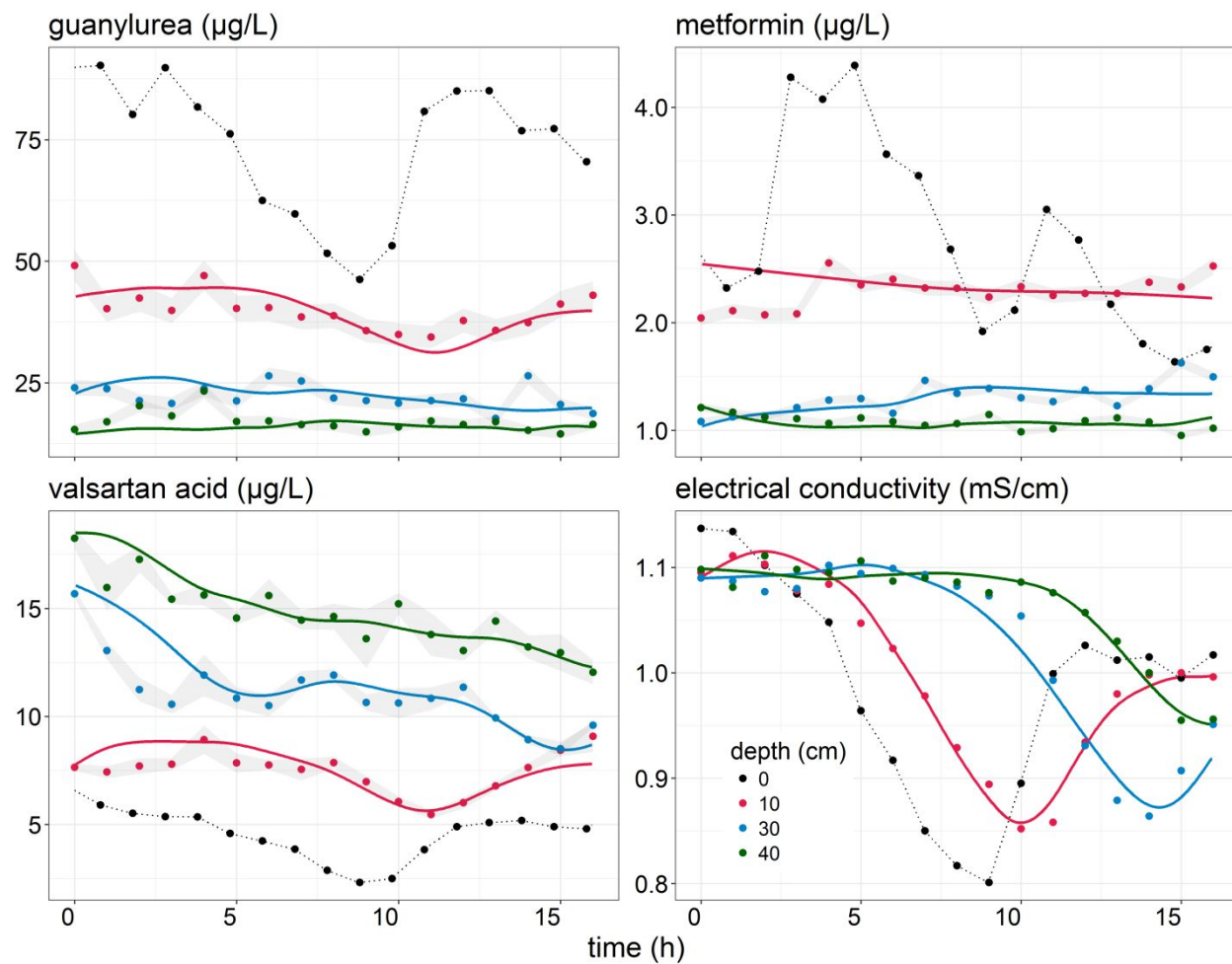
323 Although the antidiabetic drug metformin and its main TP guanylurea<sup>50</sup> have been detected ubiquitously in  
324 surface waters,<sup>51,52</sup> qualitative information on the fate of the two compounds in saturated sediments is  
325 relatively scarce. Both were found to be rather stable in laboratory batch experiments;<sup>50,53</sup> a finding that  
326 cannot be confirmed in the present study where they show half-lives in the HZ of several hours.  
327 Calculated half-lives for the beta-blockers MTP are in line with findings of a laboratory column study  
328 reporting half-lives of several hours for oxic/suboxic conditions,<sup>12</sup> but contrast results of investigations  
329 conducted previously at the same study site, in which MTP was, on average, not significantly removed  
330 along a 20 cm long hyporheic flow path.<sup>14</sup> Metoprolol acid (MTA), a main TP of MTP, was formed in the  
331 HZ, suggesting that removal of MTP in the HZ is at least in part due to transformation into MTA.  
332 Quantitative information on the fate of the beta blocker sotalol (SOT) and the opioid analgesic tramadol  
333 (TRA) in the HZ is limited. For SOT and TRA, a concentration decrease in the HZ<sup>25</sup> and in sediments of a  
334 flume study mimicking the HZ,<sup>13</sup> respectively, has been reported, but no removal rates were calculated.  
335 The antihypertensive drugs olmesartan (OLM), irbesartan (IRB), candesartan (CAN) and valsartan (VAL)  
336 were significantly removed along the investigated flow path. Simultaneously concentrations of their  
337 common TP valsartan acid<sup>54,55</sup> (VSA) increased. At least part of the removal of OLM, CAN, VAL and  
338 IRB can therefore be attributed to transformation to VSA. While VAL removal in hyporheic sediments  
339 has been described,<sup>17</sup> OLM and CAN were found to be rather stable in both, hyporheic sediments and  
340 during river bank filtration.<sup>17,49</sup> Although removal of VSA has been described in bank filtration systems,<sup>49</sup>  
341 concentrations of its PCs were likely too high in the HZ and thus net formation rates were higher than  
342 potential VSA removal rates.

343 Carbamazepine (CBZ) and one of its TPs dihydroxy-carbamazepine (DBZ), diclofenac (DCF), diatrizoic  
344 acid (diatrizoate, DTA) and venlafaxine (VLX) and its TP *O*-desmethylvenlafaxine (MLX) were not  
345 significantly removed and were thus considered to be rather stable along the investigated flow path (Table  
346 2). CBZ is well known for its stability in saturated sediments<sup>56</sup> and hitherto, removal has only been  
347 observed under iron-reducing conditions after long (several days) residence times.<sup>57</sup> Since concentrations

348 of DBZ remained relatively constant along the investigated flow path it is reasonable to assume that  
349 transformation of CBZ to DBZ along short (<40 cm) and rather oxic flow paths in the HZ is limited.  
350 Laboratory and field studies have demonstrated that VLX,<sup>58</sup> DCF<sup>12,14</sup> and DTA<sup>59</sup> can be removed in  
351 saturated sediments. It is therefore likely that in the present study exposure times to favorable  
352 biogeochemical conditions in the HZ times were likely too short to facilitate significant removal of these  
353 compounds.

354 The anticonvulsant primidone (PRI) and the antibiotic sulfamethoxazole (SMX) showed negative removal  
355 indicating a concentration increase in the HZ. To the best of our knowledge, formation of PRI in the HZ  
356 has not been reported and we thus attribute the small concentration increase ( $18\pm 7\%$ ) to desorption  
357 processes. For SMX however, back-transformation of photo-transformation products into SMX has been  
358 observed in water/sediment systems.<sup>60</sup> It is therefore perceivable that back-transformation was responsible  
359 for the observed concentration increase of SMX. The TrOC 4-formylaminoantipyrin (FAA), a human  
360 metabolite of metamizole<sup>61</sup> (a phenazone-type analgesics not investigated in the present study), was found  
361 to be removed between 0 and 30 cm depth but was formed between 30 and 40 cm depth. Removal of FAA  
362 in oxic sections of saturated sediments has been described,<sup>12,62</sup> although a previous investigation at the  
363 same site found inconsistent behavior (removal in some profiles, formation in others) of the compound.<sup>14</sup>  
364 It remains unclear whether the formation of FAA during suboxic (i.e. denitrifying) redox conditions is due  
365 to back-transformation or due to increased transformation of its PC(s).

366 For some compounds (e.g. OLM), modeled concentration time series could be fitted well over the entire  
367 time series. For other compounds such as MTP, VSA or GUA (Figure 1, Figure SI-24), modeled  
368 concentrations matched measured concentration time series well in some parts of the time series but  
369 deviated in others. Such discrepancies indicate that model assumptions such as time invariant porewater  
370 velocities or removal rate constants were not met throughout the sampling event. Time varying removal  
371 rate constants could be the consequence of temperature dependent biotransformation rates or varying  
372 substrate and TrOC concentrations in the surface water.



373

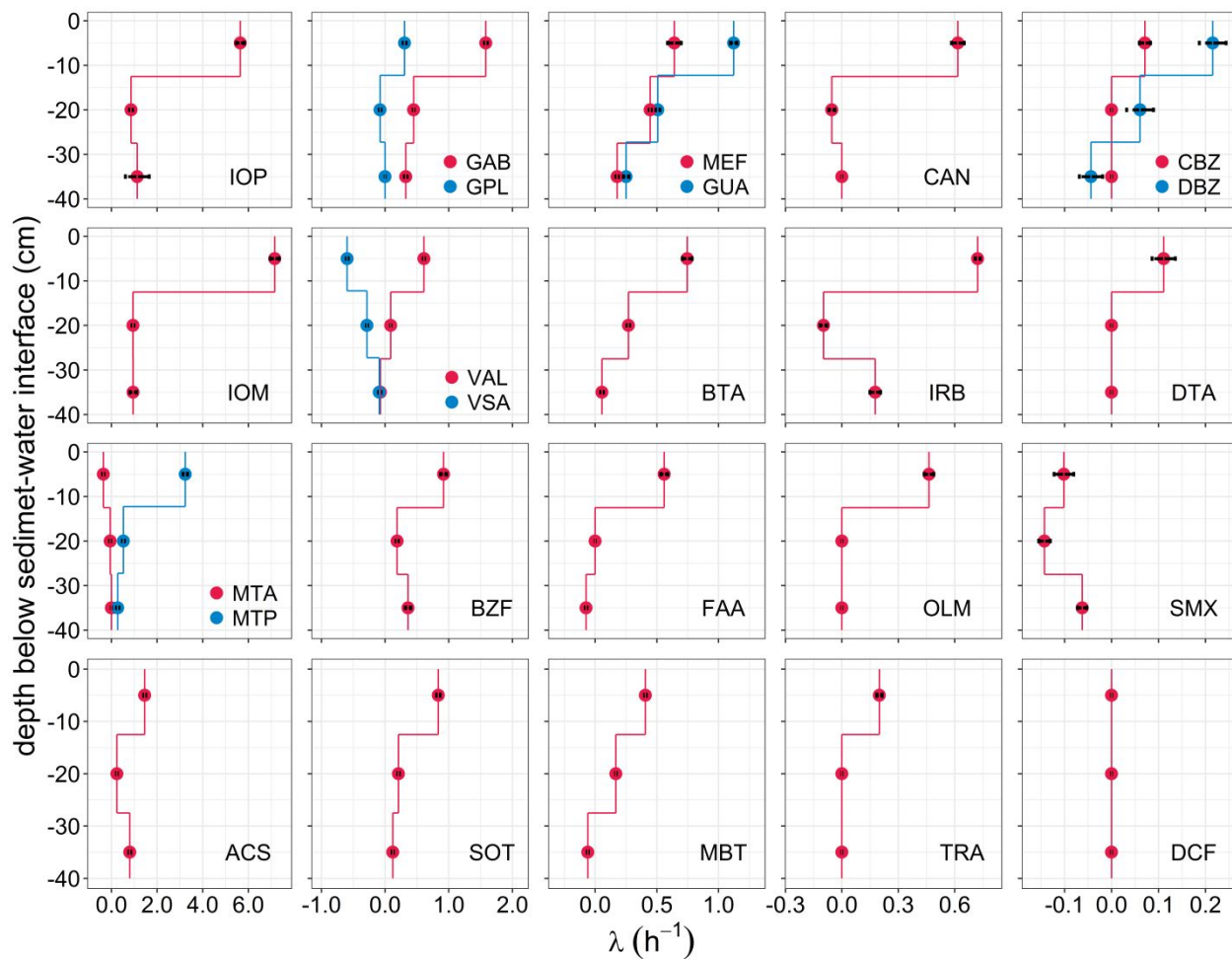
374 **Figure 2** Measured (dots) and modeled (solid lines) concentration time series in 10 cm, 30 cm and 40 cm depth in the hyporheic  
 375 zone (HZ) and measured concentration time series in the surface water (0 cm) of guanylurea (GUA), metformin (MEF), valsartan  
 376 acid (VSA) and electrical conductivity (EC). For concentration time series measured in the HZ, analytical uncertainty (one  
 377 standard deviation) is shown in grey. Note that for modeling purposes, concentration time series in the surface water were linearly  
 378 interpolated (black dashed line) and that for EC no measurement uncertainties were available.

379

380 **Table 2** Relative removal in the upper 40 cm of the hyporheic zone ( $Rel_x^{0-40}$ , %), half-lives ( $t_{1/2}$ , h) and retardation coefficients (R, dimensionless) of all trace organic compounds investigated in the present study except epoxy-carbamazepine calculated between  
 381 0 and 10, 10 and 30 and 30 and 40 cm depth in the hyporheic zone. Note that retardation coefficients could only be estimated  
 382 from input time series that showed a distinct temporal pattern, i.e. a trough or peak. Half-lives exceeding the sampling period (i.e.,  
 383 17 h) were set to infinity.  
 384

TrOC	$Rel_x^{0-40}$ (%)		$t_{1/2}$ (h)				R (-)	
	0-40	0-10	10-30	30-40	0-10	10-30	30-40	
acesulfame (ACS)	78±1	0.5±0.0	2.9±0.2	0.9±0.0	1.2±0.1	1.0	n.e.	
benzotriazole (BTA)	63±2	0.9±0.0	2.6±0.1	12.6±2.6*	4.0±0.5	n.e.	n.e.	
bezafibrate (BZF)	69±2	0.8±0.0	3.7±0.1	1.9±0.2	2.6±0.3	2.8±0.0	n.e.	
candesartan (CAN)	27±4	1.1±0.1	12.9±3.8 <sup>f</sup> *	inf	1.7±0.2	1.3±0.1	n.e.	
carbamazepine (CBZ)	9±5*	9.8±1.6	inf	inf	3.6±0.3	n.e.	n.e.	
dihydroxy-carbamazepine (DBZ)	-1±6*	3.2±0.4*	11.4±5.3	15.8±8.9 <sup>f</sup>	2.2±0.3	n.e.	n.e.	
diclofenac (DCF)	-11±6*	inf	inf	inf	4.3±0.3	n.e.	n.e.	
diatrizoic acid (DTA)	0±9*	6.3±1.4*	inf	inf	1.1±0.1	2.0±2.5	n.e.	
4-formylaminoantipyrine (FAA)	10±4	1.2±0.1	inf	9.4±0.9 <sup>f</sup>	2.4±0.2	1.5±0.1	n.e.	
gabapentin (GAB)	79±1	0.4±0.0	1.5±0.0	2.1±0.1	1.4±0.0	1.4±0.1	3.7±0.6	
gabapentin-lactam (GPL)	12±5	2.3±0.2	8.9±1.4 <sup>f</sup> *	inf	1.3±0.2	n.e.	n.e.	
guanyldurea (GUA)	78±1	0.6±0.0	1.4±0.0	2.8±0.3	2.6±0.2	n.e.	n.e.	
iomeprol (IOM)	98±0	0.1±0.0	0.7±0.0	0.7±0.1	1.9±0.4	1.1±0.1	n.e.	
iopromid (IOP)	98±0	0.1±0.0	0.8±0.1	0.6±0.3	n.e.	n.e.	n.e.	
irbesartan (IRB)	37±3	1.0±0.0	7.1±1.3 <sup>f</sup>	3.9±0.6	3.5±0.1	n.e.	n.e.	
methylbenzotriazole (MBT)	36±3	1.7±0.0	4.1±0.1	11.6±0.9 <sup>f</sup>	3.3±0.1	n.e.	n.e.	
metformin (MEF)	66±2	1.1±0.1	1.6±0.0	3.9±0.2	15.3±2.2	n.e.	n.e.	
O-desmethylvenlafaxine (MLX)	0±6*	14.1±6.8 <sup>f</sup>	12.1±5.6*	inf	1.5±0.2	n.e.	n.e.	
metoprolol acid (MTA)	-35±8	2.0±0.2 <sup>f</sup>	12.8±4.7 <sup>f</sup> *	inf	n.e.	n.e.	n.e.	
metoprolol (MTP)	90±1	0.2±0.0	1.3±0.1	2.5±0.5	4.5±0.5	n.e.	n.e.	
olmesartan (OLM)	18±4	1.5±0.1	inf	inf	1.4±0.1	1.3±0.2	n.e.	
primidone (PRI)	-18±7	10.3±3.9 <sup>f</sup> *	inf	11.0±0.8 <sup>f</sup> *	1.4±0.1	n.e.	n.e.	
sulfamethoxazole (SMX)	-47±8	6.8±1.4 <sup>f</sup> *	4.9±0.4 <sup>f</sup>	11.1±1.7 <sup>f</sup> *	1.6±0.2	1.1±0.1	1.1±0.1	
sotalol (SOT)	50±2	0.8±0.0	3.3±0.2	5.8±0.6*	1.9±0.2	n.e.	n.e.	
tramadol (TRA)	12±4	3.5±0.2	inf	inf	2.2±0.2	n.e.	n.e.	
valsartan (VAL)	26±4	1.1±0.0	7.8±0.2	9.4±1.1 <sup>f</sup> *	1.9±0.0	n.e.	n.e.	
venlafaxine (VLX)	-5±9*	6.2±2.2*	inf	9.0±5.8*	3.6±0.6	n.e.	n.e.	
valsartan acid (VSA)	-205±15	1.2±0.0 <sup>f</sup>	2.4±0.1 <sup>f</sup>	7.6±0.9 <sup>f</sup>	1.1±0.1	1.0±0.0	n.e.	

385 inf = half-life > 17 h. \* = not significantly removed/formed as indicated by  $Rel_x$ . n.e. = not estimated. f = TrOC formation.



386

387 **Figure 3** First-order removal rate constants ( $\lambda$ ) as a function of depth of all investigated parent compounds (PCs, shown in red)  
 388 and transformation compounds (TPs, shown in blue) except, primidone, epoxy-carbamazepine, venlafaxine and *O*-  
 389 desmethylvenlafaxine. Error bars indicate one standard deviation. ACS, acesulfame; BTA, benzotriazole; BZF, bezafibrate; CAN,  
 390 candesartan; CBZ, carbamazepine; DBZ, dihydroxy-carbamazepine; DCF, diclofenac; DTA, diatrizoic acid; FAA, 4-  
 391 formylaminoantipyrine; GAB, gabapentin; GPL, gabapentin-lactam; GUA, guanylurea; IOM, iomeprol; IOP, iopromide; IRB,  
 392 irbesartan; MBT, methylbenzotriazole; MEF, metformin; MTA, metoprolol acid; MTP, metoprolol; olmesartan, OLM; SMX,  
 393 sulfamethoxazole; SOT, sotalol; TRA, tramadol; VAL, valsartan; VSA, valsartan acid.

394

### 395 **3.4 Retardation of TrOCs in the HZ**

396 Surface water concentration time series of all 28 TrOCs that were further investigated in the present study  
397 showed a pronounced temporal pattern (i.e. a concentration trough) and thus retardation coefficients for all  
398 TrOCs except IOP and MTA could be calculated for the first 10 cm in the HZ. However, concentration  
399 time series of many TrOCs measured in 10 and 30 cm did no longer exhibit a distinct temporal pattern and  
400 thus retardation coefficients could not be estimated between 10 - 30 and 30 - 40 cm for these compounds  
401 (Table 2). Calculated retardation coefficients ranged from  $1.1 \pm 0.1$  (i.e., no retardation) for compounds  
402 such as ACS, VSA, and DTA to  $15.3 \pm 2.2$  for MEF (Table 2).

403 Retardation of TrOCs along hyporheic flow paths is due to reversible sorption processes caused by a  
404 variety of interaction mechanisms between TrOCs and streambed sediments and biofilms. Neutral TrOCs  
405 interact with streambed materials predominately via hydrophobic partitioning, while sorption and  
406 retardation of ionizable compounds can additionally be caused by electrostatic interactions and surface  
407 complexation.<sup>18</sup> At ambient pH values measured in River Erpe during the sampling campaign ( $\text{pH} \approx 7.3$ ),  
408 7 of the investigated compounds occur as cations (GUA, MEF, MTP, SOT, VLX, MLX and TRA), 10  
409 TrOCs occur as anions (ACS, BZF, CAN, DCF, DTA, IRB, OLM, SMX, VAL and VSA), 2 occur as a  
410 zwitterions (GAB, MTA) and 9 do not carry any charge (BTA, CBZ, DBZ, FAA, GPL, IOM, IOP, MBT,  
411 and PRI). To assess the possible influence of hydrophobic partitioning retardation, Pearson Product  
412 Moment correlations were calculated between retardation coefficients estimated for the first 10 cm in the  
413 HZ and pH-dependent octanol-water partitioning coefficients ( $\log D_{ow}$ ) of the respective TrOCs (obtained  
414 from [www.chemicalize.com](http://www.chemicalize.com), Table SI-05). Retardation coefficients of positively charged TrOCs were all  
415 larger than 1 and did not significantly correlate with  $\log D_{ow}$  values (Table SI-06), suggesting that the  
416 contribution of hydrophobic partitioning to retardation of cationic TrOCs is negligible. This finding is in  
417 line with previous observations indicating that sorption of cationic TrOCs, such as MEF, its TP GUA,<sup>63</sup>  
418 VLX<sup>64</sup> and beta-blockers such as MTP and SOT<sup>13,65</sup> to sediment materials can be substantial and occurs  
419 predominately via electrostatic interactions. By contrast,  $\log D_{ow}$  values of negatively charged TrOCs

420 correlated positively with estimated retardation coefficients (Table SI-06), indicating that retardation of  
421 anionic TrOCs in the HZ is at least partially caused by hydrophobic partitioning into sediment organic  
422 matter. This finding is in agreement with work that showed that sorption of anionic compounds is driven  
423 by their hydrophobicity rather than by electrostatic interactions.<sup>66</sup> For the neutral TrOCs PRI, CBZ, and  
424 DBZ, retardation coefficients found in a laboratory column ( $R_{CBZ} = 2.1$ ,  $R_{DBZ} = 3.2$ ,  $f_{oc} = 0.29\%$ )<sup>20</sup> and  
425 batch tests ( $R_{CBZ} = 3.6-5.3$ ,  $R_{PRI} = 1.2$ ,  $f_{oc} = 0.23\%$ )<sup>21</sup> compared well to values calculated in the present  
426 study (sediment  $f_{oc} = 0.5 - 6\%$ ),<sup>14</sup> while a field study had found negligible retardation for compounds such  
427 as CBZ and BTA during riparian bank filtration ( $f_{oc} = 0.01-0.11\%$ ).<sup>16</sup> Such discrepancies are likely  
428 attributable to differences in sediment organic matter content and general sediment heterogeneity.

429 We conclude that reversible sorption processes can substantially retard TrOCs along hyporheic flow paths,  
430 even for compounds that are negatively charged. Retardation caused by reversible sorption processes  
431 increases the residence time of TrOCs relative to the water residence time in the HZ. Neglecting the effect  
432 of retardation may lead to erroneous estimates of removal rate constants, particularly when their  
433 calculation is based on simple concentration differences<sup>17</sup> and when sampling periods are relatively short  
434 compared to the characteristic time scales over which surface water concentrations fluctuate. Studies that  
435 aim at quantitatively investigating the fate of TrOCs in the HZ and along river reaches with significant  
436 hyporheic exchange flows should therefore consider retardation and adjust their reactive transport models  
437 and sampling schemes accordingly. Some compounds (e.g. CBZ, DBZ, VLX, or DCF) were retarded  
438 along the investigated hyporheic flow path but showed only very small removal rates in the HZ. If  
439 concentrations of these compounds in surface waters drop considerably over short time scales (e.g. during  
440 hydrological events), desorption processes might remobilize TrOCs previously adsorbed to sediment  
441 materials and biofilms and hence hyporheic exchange would lead to a concentration increase of these  
442 TrOCs in the surface water.

443

### 444 **3.5 Influence of benthic bio-layer and DOC on TrOC reactivity**

445 For all TrOCs for which concentration changed significantly between the surface water and 40 cm depth  
446 in the HZ (22 out of 28) except SMX, removal rates calculated for the top 10 cm in the HZ were  
447 substantially higher compared to removal rate constants calculated between 10 and 30 and 30 and 40 cm  
448 depth (Figure 3). Because redox conditions in the top 30 cm of the HZ were predominantly oxic, it is  
449 reasonable to assume that the increased reactivity in the top 10 cm of the HZ is due to increased microbial  
450 activity in the benthic bio-layers growing in the top cm of the HZ and high chemical turnover rates  
451 typically associated with shallow hyporheic flow paths.<sup>10,11</sup> This finding is further underlined by changes  
452 in DOC concentration and quality, suggesting that TrOC turnover within similar redox zones in the HZ is  
453 closely coupled to DOC turnover. Studies on managed aquifer recharge reported that TrOC removal rates  
454 under oxic conditions were highest when BDOC was limited, an observation that was mainly attributed to  
455 the presence of highly adapted microbial communities that developed under oligotrophic conditions.<sup>22,49,67</sup>  
456 However, our results show, that in natural systems such as the HZ, high TrOC removal rates can also be  
457 associated with oxic and eutrophic conditions, in which high concentrations of BDOC likely fuel  
458 microbial metabolism and serve as a co-substrate for the co-metabolic removal of TrOCs.  
459 Due to practical limitations associated with our sampling approach, the present study investigated a  
460 downwelling flow path that is unlikely to return to the surface water. However, our findings should in  
461 principle be transferable to hyporheic flow paths that return to the stream and thus have implications for  
462 reach-scale removal of TrOCs. Together with earlier investigations showing that for many TrOCs removal  
463 rates are higher under oxic compared to anoxic redox conditions,<sup>12,14</sup> our results suggest that short and  
464 shallow flow paths are more efficient in removing TrOCs than long and deep flow paths, along which  
465 redox conditions become increasingly anoxic and microbial activity decreases. River restoration measures  
466 that promote frequent and short vertical exchange flows through the shallow HZ, such as the construction  
467 of engineered hyporheic zone elements<sup>68-70</sup> or the application of woody debris,<sup>71</sup> are therefore likely to

468 contribute more to overall in-stream removal of TrOCs than measures that promote, longer lateral  
469 exchange flows such as the installation of meander bends or pool-riffle sequences.

470

471 **References**

- 472 (1) Ternes, T. A.; Joss, A.; Siegrist, H. Peer Reviewed: Scrutinizing Pharmaceuticals and Personal  
473 Care Products in Wastewater Treatment. *Environ. Sci. Technol.* **2004**, *38* (20), 392A–399A.  
474 <https://doi.org/10.1021/es040639t>.
- 475 (2) Eggen, R. I. L.; Hollender, J.; Joss, A.; Schärer, M.; Stamm, C. Reducing the Discharge of  
476 Micropollutants in the Aquatic Environment: The Benefits of Upgrading Wastewater Treatment  
477 Plants. *Environ. Sci. Technol.* **2014**, *48* (14), 7683–7689. <https://doi.org/10.1021/es500907n>.
- 478 (3) Bradley, P. M.; Journey, C. A.; Romanok, K. M.; Barber, L. B.; Buxton, H. T.; Foreman, W. T.;  
479 Furlong, E. T.; Glassmeyer, S. T.; Hladik, M. L.; Iwanowicz, L. R.; Jones, D. K.; Kolpin, D. W.;  
480 Kuivila, K. M.; Loftin, K. A.; Mills, M. A.; Meyer, M. T.; Orlando, J. L.; Reilly, T. J.; Smalling,  
481 K. L.; Villeneuve, D. L. Expanded Target-Chemical Analysis Reveals Extensive Mixed-Organic-  
482 Contaminant Exposure in U.S. Streams. *Environ. Sci. Technol.* **2017**, *51* (9), 4792–4802.  
483 <https://doi.org/10.1021/acs.est.7b00012>.
- 484 (4) Loos, R.; Carvalho, R.; António, D. C.; Comero, S.; Locoro, G.; Tavazzi, S.; Paracchini, B.;  
485 Ghiani, M.; Lettieri, T.; Blaha, L.; Jarosova, B.; Voorspoels, S.; Servaes, K.; Haglund, P.; Fick, J.;  
486 Lindberg, R. H.; Schwesig, D.; Gawlik, B. M. EU-Wide Monitoring Survey on Emerging Polar  
487 Organic Contaminants in Wastewater Treatment Plant Effluents. *Water Res.* **2013**, *47* (17), 6475–  
488 6487. <https://doi.org/10.1016/j.watres.2013.08.024>.
- 489 (5) Brodin, T.; Fick, J.; Jonsson, M.; Klaminder, J. Dilute Concentrations of a Psychiatric Drug Alter  
490 Behavior of Fish from Natural Populations. *Science* **2013**, *339* (6121), 814–815.  
491 <https://doi.org/10.1126/science.1226850>.
- 492 (6) Schwarzenbach, R. P.; Egli, T.; Hofstetter, T. B.; von Gunten, U.; Wehrli, B. Global Water  
493 Pollution and Human Health. *Annu. Rev. Environ. Resour.* **2010**, *35* (1), 109–136.  
494 <https://doi.org/10.1146/annurev-environ-100809-125342>.
- 495 (7) Arnnok, P.; Singh, R. R.; Burakham, R.; Pérez-Fuentetaja, A.; Aga, D. S. Selective Uptake and

- 496 Bioaccumulation of Antidepressants in Fish from Effluent-Impacted Niagara River. *Environ. Sci.*  
497 *Technol.* **2017**, *51* (18), 10652–10662. <https://doi.org/10.1021/acs.est.7b02912>.
- 498 (8) Pal, A.; He, Y.; Jekel, M.; Reinhard, M.; Gin, K. Y. H. Emerging Contaminants of Public Health  
499 Significance as Water Quality Indicator Compounds in the Urban Water Cycle. *Environment*  
500 *International*. 2014, *71*, 46–62. <https://doi.org/10.1016/j.envint.2014.05.025>.
- 501 (9) Boano, F.; Harvey, J. W.; Marion, A.; Packman, A. I.; Revelli, R.; Ridolfi, L.; Wörman, A.  
502 Hyporheic Flow and Transport Processes: Mechanisms, Models, and Biogeochemical Implications.  
503 *Rev. Geophys.* **2014**, *52*, 603–379. <https://doi.org/10.1002/2012RG000417>.Received.
- 504 (10) Knapp, J. L. A.; González-Pinzón, R.; Drummond, J. D.; Larsen, L. G.; Cirpka, O. A.; Harvey, J.  
505 W. Tracer-Based Characterization of Hyporheic Exchange and Benthic Biolayers in Streams.  
506 *Water Resour. Res.* **2017**, *53*, 1575–1594. <https://doi.org/10.1002/2016WR019393>.
- 507 (11) Krause, S.; Lewandowski, J.; Grimm, N. B.; Hannah, D. M.; Pinay, G.; McDonald, K.; Martí, E.;  
508 Argerich, A.; Pfister, L.; Klaus, J.; Battin, T.; Larned, S. T.; Schelker, J.; Fleckenstein, J.; Schmidt,  
509 C.; Rivett, M. O.; Watts, G.; Sabater, F.; Sorolla, A.; Turk, V. Ecohydrological Interfaces as Hot  
510 Spots of Ecosystem Processes. *Water Resour. Res.* **2017**, *53* (8), 6359–6376.  
511 <https://doi.org/10.1002/2016WR019516>.
- 512 (12) Burke, V.; Greskowiak, J.; Asmuß, T.; Bremermann, R.; Taute, T.; Massmann, G. Temperature  
513 Dependent Redox Zonation and Attenuation of Wastewater-Derived Organic Micropollutants in  
514 the Hyporheic Zone. *Sci. Total Environ.* **2014**, *482–483* (1), 53–61.  
515 <https://doi.org/10.1016/j.scitotenv.2014.02.098>.
- 516 (13) Li, Z.; Sobek, A.; Radke, M. Flume Experiments to Investigate the Environmental Fate of  
517 Pharmaceuticals and Their Transformation Products in Streams. *Environ. Sci. Technol.* **2015**, *49*  
518 (10), 6009–6017. <https://doi.org/10.1021/acs.est.5b00273>.
- 519 (14) Schaper, J. L.; Seher, W.; Nützmann, G.; Putschew, A.; Jekel, M.; Lewandowski, J. The Fate of  
520 Polar Trace Organic Compounds in the Hyporheic Zone. *Water Res.* **2018**, *140*, 158–166.

- 521 <https://doi.org/10.1016/j.watres.2018.04.040>.
- 522 (15) Lewandowski, J.; Putschew, A.; Schwesig, D.; Neumann, C.; Radke, M. Fate of Organic  
523 Micropollutants in the Hyporheic Zone of a Eutrophic Lowland Stream: Results of a Preliminary  
524 Field Study. *Sci. Total Environ.* **2011**, *409* (10), 1824–1835.  
525 <https://doi.org/10.1016/j.scitotenv.2011.01.028>.
- 526 (16) Huntscha, S.; Rodriguez Velosa, D. M.; Schroth, M. H.; Hollender, J. Degradation of Polar  
527 Organic Micropollutants during Riverbank Filtration: Complementary Results from Spatiotemporal  
528 Sampling and Push-Pull Tests. *Environ. Sci. Technol.* **2013**, *47* (20), 11512–11521.  
529 <https://doi.org/10.1021/es401802z>.
- 530 (17) Schaper, J. L.; Posselt, M.; McCallum, J. L.; Banks, E.; Hoehne, A.; Meinikmann, K.; Shanafield,  
531 M.; Batelaan, O.; Lewandowski, J. Hyporheic Exchange Controls Fate of Trace Organic  
532 Compounds in an Urban Stream. *Environ. Sci. Technol.* **2018**, *52*, 12285–12294.  
533 <https://doi.org/10.1021/acs.est.8b03117>.
- 534 (18) MacKay, A. A.; Vasudevan, D. Polyfunctional Ionogenic Compound Sorption: Challenges and  
535 New Approaches to Advance Predictive Models. *Environ. Sci. Technol.* **2012**, *46* (17), 9209–9223.  
536 <https://doi.org/10.1021/es301036t>.
- 537 (19) Schaffer, M.; Börnick, H.; Nödler, K.; Licha, T.; Worch, E. Role of Cation Exchange Processes on  
538 the Sorption Influenced Transport of Cationic  $\beta$ -Blockers in Aquifer Sediments. *Water Res.* **2012**,  
539 *46* (17), 5472–5482. <https://doi.org/10.1016/j.watres.2012.07.013>.
- 540 (20) Writer, J. H.; Antweiler, R. C.; Ferrer, I.; Ryan, J. N.; Thurman, E. M. In-Stream Attenuation of  
541 Neuro-Active Pharmaceuticals and Their Metabolites. *Environ. Sci. Technol.* **2013**, *47* (17), 9781–  
542 9790. <https://doi.org/10.1021/es402158t>.
- 543 (21) Schaffer, M.; Boxberger, N.; Börnick, H.; Licha, T.; Worch, E. Sorption Influenced Transport of  
544 Ionizable Pharmaceuticals onto a Natural Sandy Aquifer Sediment at Different PH. *Chemosphere*  
545 **2012**, *87* (5), 513–520. <https://doi.org/10.1016/j.chemosphere.2011.12.053>.

- 546 (22) Rauch-Williams, T.; Hoppe-Jones, C.; Drewes, J. E. The Role of Organic Matter in the Removal of  
547 Emerging Trace Organic Chemicals during Managed Aquifer Recharge. *Water Res.* **2010**, *44* (2),  
548 449–460. <https://doi.org/10.1016/j.watres.2009.08.027>.
- 549 (23) Harvey, J. W.; Böhlke, J. K.; Voytek, M. A.; Scott, D.; Tobias, C. R. Hyporheic Zone  
550 Denitrification: Controls on Effective Reaction Depth and Contribution to Whole-Stream Mass  
551 Balance. *Water Resour. Res.* **2013**, *49* (10), 6298–6316. <https://doi.org/10.1002/wrcr.20492>.
- 552 (24) Peralta-Maraver, I.; Galloway, J.; Posselt, M.; Arnon, S.; Reiss, J.; Lewandowski, J.; Robertson, A.  
553 L. Environmental Filtering and Community Delineation in the Streambed Ecotone. *Sci. Rep.* **2018**,  
554 *8* (October 2017), 1–11. <https://doi.org/10.1038/s41598-018-34206-z>.
- 555 (25) Kunkel, U.; Radke, M. Fate of Pharmaceuticals in Rivers: Deriving a Benchmark Dataset at  
556 Favorable Attenuation Conditions. *Water Res.* **2012**, *46* (17), 5551–5565.  
557 <https://doi.org/10.1016/j.watres.2012.07.033>.
- 558 (26) Posselt, M.; Jaeger, A.; Schaper, J. L.; Radke, M.; Benskin, J. P. Determination of Polar Organic  
559 Micropollutants in Surface and Pore Water by High-Resolution Sampling-Direct Injection-Ultra  
560 High Performance Liquid Chromatography-Tandem Mass Spectrometry. *Environ. Sci. Process.*  
561 *Impacts* **2018**, *20* (12), 1716–1727. <https://doi.org/10.1039/c8em00390d>.
- 562 (27) Munz, M.; Oswald, S. E.; Schmidt, C. Analysis of Riverbed Temperatures to Determine the  
563 Geometry of Subsurface Water Flow around In-Stream Geomorphological Structures. *J. Hydrol.*  
564 **2016**, *539*, 74–87. <https://doi.org/10.1016/j.jhydrol.2016.05.012>.
- 565 (28) McCallum, A. M.; Andersen, M. S.; Rau, G. C.; Acworth, R. I. A 1-D Analytical Method for  
566 Estimating Surface Water-Groundwater Interactions and Effective Thermal Diffusivity Using  
567 Temperature Time Series. *Water Resour. Res.* **2012**, *48* (11), 1–8.  
568 <https://doi.org/10.1029/2012WR012007>.
- 569 (29) Gordon, R. P.; Lautz, L. K.; Briggs, M. A.; McKenzie, J. M. Automated Calculation of Vertical  
570 Pore-Water Flux from Field Temperature Time Series Using the VFLUX Method and Computer

- 571 Program. *J. Hydrol.* **2012**, *420–421*, 142–158. <https://doi.org/10.1016/j.jhydrol.2011.11.053>.
- 572 (30) Young, P. C.; Pedregal, D. J.; Tych, W. Dynamic Harmonic Regression. *J. Forecast.* **1999**, *18* (6),  
573 369–394. [https://doi.org/10.1002/\(SICI\)1099-131X\(199911\)18:6<369::AID-FOR748>3.0.CO;2-K](https://doi.org/10.1002/(SICI)1099-131X(199911)18:6<369::AID-FOR748>3.0.CO;2-K).
- 574 (31) Jaeger, A.; Posselt, M.; Betterle, A.; Schaper, J.; Mechelke, J.; Coll, C.; Lewandowski, J. Spatial  
575 and Temporal Variability in Attenuation of Polar Organic Micropollutants in an Urban Lowland  
576 Stream. *Environ. Sci. Technol.* **2018**, *53*, 2383–2395. <https://doi.org/10.1021/acs.est.8b05488>.
- 577 (32) Zietzschmann, F.; Aschermann, G.; Jekel, M. Comparing and Modeling Organic Micro-Pollutant  
578 Adsorption onto Powdered Activated Carbon in Different Drinking Waters and WWTP Effluents.  
579 *Water Res.* **2016**, *102*, 190–201. <https://doi.org/10.1016/j.watres.2016.06.041>.
- 580 (33) Aschermann, G.; Zietzschmann, F.; Jekel, M. Influence of Dissolved Organic Matter and Activated  
581 Carbon Pore Characteristics on Organic Micropollutant Desorption. *Water Res.* **2018**, *133*, 123–  
582 131. <https://doi.org/10.1016/j.watres.2018.01.015>.
- 583 (34) Ohno, T. Fluorescence Inner-Filtering Correction for Determining the Humification Index of  
584 Dissolved Organic Matter. *Environ. Sci. Technol.* **2002**, *36* (4), 742–746.  
585 <https://doi.org/10.1021/es0155276>.
- 586 (35) Weishaar, J. L.; Aiken, G. R.; Bergamaschi, B. A.; Fram, M. S.; Fujii, R.; Mopper, K. Evaluation  
587 of Specific Ultraviolet Absorbance as an Indicator of the Chemical Composition and Reactivity of  
588 Dissolved Organic Carbon. *Environ. Sci. Technol.* **2003**, *37* (20), 4702–4708.  
589 <https://doi.org/10.1021/es030360x>.
- 590 (36) Harvey, R. W.; Garabedian, S. P. Use of Colloid Filtration Theory in Modelling Movement of  
591 Bacteria through a Contaminated Sandy Aquifer. *Environ. Sci. Technol.* **1991**, *25*, 178–185.
- 592 (37) Kunkel, U.; Radke, M. Reactive Tracer Test to Evaluate the Fate of Pharmaceuticals in Rivers.  
593 *Environ. Sci. Technol.* **2011**, *45* (15), 6296–6302. <https://doi.org/10.1021/es104320n>.
- 594 (38) Vrugt, J. A.; Robinson, B. A.; Clark, M. P.; ter Braak, C. J. F.; Hyman, J. M. Treatment of Input  
595 Uncertainty in Hydrologic Modeling: Doing Hydrology Backward with Markov Chain Monte

- 596 Carlo Simulation. *Water Resour. Res.* **2008**, *44* (12), 1–15. <https://doi.org/10.1029/2007wr006720>.
- 597 (39) Vrugt, J. A. Markov Chain Monte Carlo Simulation Using the DREAM Software Package: Theory,  
598 Concepts, and MATLAB Implementation. *Environ. Model. Softw.* **2016**, *75*, 273–316.  
599 <https://doi.org/10.1016/j.envsoft.2015.08.013>.
- 600 (40) Voermans, J. J.; Ghisalberti, M.; Ivey, G. N. A Model for Mass Transport Across the Sediment-  
601 Water Interface. *Water Resour. Res.* **2018**, *54* (4), 2799–2812.  
602 <https://doi.org/10.1002/2017WR022418>.
- 603 (41) Grant, S. B.; Azizian, M.; Cook, P.; Boano, F.; Rippy, M. A. Factoring Stream Turbulence into  
604 Global Assessments of Nitrogen Pollution. *Science* **2018**, *359*, 1266–1269.
- 605 (42) Zarnetske, J. P.; Haggerty, R.; Wondzell, S. M.; Baker, M. A. Dynamics of Nitrate Production and  
606 Removal as a Function of Residence Time in the Hyporheic Zone. *J. Geophys. Res. Biogeosciences*  
607 **2011**, *116* (1), 1–12. <https://doi.org/10.1029/2010JG001356>.
- 608 (43) Mulholland, P. J.; Helton, A. M.; Poole, G. C.; Hall, R. O.; Hamilton, S. K.; Peterson, B. J.; Tank,  
609 J. L.; Ashkenas, L. R.; Cooper, L. W.; Dahm, C. N.; Dodds, W. K.; Findlay, S. E. G.; Gregory, S.  
610 V.; Grimm, N. B.; Johnson, S. L.; McDowell, W. H.; Meyer, J. L.; Valett, H. M.; Webster, J. R.;  
611 Arango, C. P.; Beaulieu, J. J.; Bernot, M. J.; Burgin, A. J.; Crenshaw, C. L.; Johnson, L. T.;  
612 Niederlehner, B. R.; O'Brien, J. M.; Potter, J. D.; Sheibley, R. W.; Sobota, D. J.; Thomas, S. M.  
613 Stream Denitrification across Biomes and Its Response to Anthropogenic Nitrate Loading. *Nature*  
614 **2008**, *452* (7184), 202–205. <https://doi.org/10.1038/nature06686>.
- 615 (44) Briggs, M. A.; Day-Lewis, F. D.; Zarnetske, J. P.; Harvey, J. W. A Physical Explanation for the  
616 Development of Redox Microzones in Hyporheic Flow. *Geophys. Res. Lett.* **2015**, *42* (11), 4402–  
617 4410. <https://doi.org/10.1002/2015GL064200>.
- 618 (45) Redeker, M.; Wick, A.; Meermann, B.; Ternes, T. A. Anaerobic Transformation of the Iodinated  
619 X-Ray Contrast Medium Iopromide, Its Aerobic Transformation Products, and Transfer to Further  
620 Iodinated X-Ray Contrast Media. *Environ. Sci. Technol.* **2018**, *52*, 8309–8320.

- 621 <https://doi.org/10.1021/acs.est.8b01140>.
- 622 (46) Schulz, M.; Löffler, D.; Wagner, M.; Ternes, T. A. Transformation of the X-Ray Contrast Medium  
623 Iopromide in Soil and Biological Wastewater Treatment. *Environ. Sci. Technol.* **2008**, *42* (19),  
624 7207–7217. <https://doi.org/10.1021/es800789r>.
- 625 (47) Kormos, J. L.; Schulz, M.; Kohler, H. P. E.; Ternes, T. A. Biotransformation of Selected Iodinated  
626 X-Ray Contrast Media and Characterization of Microbial Transformation Pathways. *Environ. Sci.*  
627 *Technol.* **2010**, *44* (13), 4998–5007. <https://doi.org/10.1021/es1007214>.
- 628 (48) Henning, N.; Kunkel, U.; Wick, A.; Ternes, T. A. Biotransformation of Gabapentin in Surface  
629 Water Matrices under Different Redox Conditions and the Occurrence of One Major TP in the  
630 Aquatic Environment. *Water Res.* **2018**, *137*, 290–300.  
631 <https://doi.org/10.1016/j.watres.2018.01.027>.
- 632 (49) Hellauer, K.; Karakurt, S.; Sperlich, A.; Burke, V.; Massmann, G.; Hübner, U.; Drewes, J. E.  
633 Establishing Sequential Managed Aquifer Recharge Technology (SMART) for Enhanced Removal  
634 of Trace Organic Chemicals: Experiences from Field Studies in Berlin, Germany. *J. Hydrol.* **2018**,  
635 *563*, 1161–1168. <https://doi.org/10.1016/j.jhydrol.2017.09.044>.
- 636 (50) Trautwein, C.; Kümmerer, K. Incomplete Aerobic Degradation of the Antidiabetic Drug  
637 Metformin and Identification of the Bacterial Dead-End Transformation Product Guanylurea.  
638 *Chemosphere* **2011**, *85* (5), 765–773. <https://doi.org/10.1016/j.chemosphere.2011.06.057>.
- 639 (51) Trautwein, C.; Berset, J. D.; Wolschke, H.; Kümmerer, K. Occurrence of the Antidiabetic Drug  
640 Metformin and Its Ultimate Transformation Product Guanylurea in Several Compartments of the  
641 Aquatic Cycle. *Environ. Int.* **2014**, *70*, 203–212. <https://doi.org/10.1016/j.envint.2014.05.008>.
- 642 (52) Bradley, P. M.; Journey, C. A.; Button, D. T.; Carlisle, D. M.; Clark, J. M.; Mahler, B. J.;  
643 Nakagaki, N.; Qi, S. L.; Waite, I. R.; VanMetre, P. C. Metformin and Other Pharmaceuticals  
644 Widespread in Wadeable Streams of the Southeastern United States. *Environ. Sci. Technol. Lett.*  
645 **2016**, *3* (6), 243–249. <https://doi.org/10.1021/acs.estlett.6b00170>.

- 646 (53) Scheurer, M.; Michel, A.; Brauch, H. J.; Ruck, W.; Sacher, F. Occurrence and Fate of the  
647 Antidiabetic Drug Metformin and Its Metabolite Guanylurea in the Environment and during  
648 Drinking Water Treatment. *Water Res.* **2012**, *46* (15), 4790–4802.  
649 <https://doi.org/10.1016/j.watres.2012.06.019>.
- 650 (54) Letzel, T.; Bayer, A.; Schulz, W.; Heermann, A.; Lucke, T.; Greco, G.; Grosse, S.; Schüssler, W.;  
651 Sengl, M.; Letzel, M. LC-MS Screening Techniques for Wastewater Analysis and Analytical Data  
652 Handling Strategies: Sartans and Their Transformation Products as an Example. *Chemosphere*  
653 **2015**, *137*, 198–206. <https://doi.org/10.1016/j.chemosphere.2015.06.083>.
- 654 (55) Nödler, K.; Hillebrand, O.; Idzik, K.; Strathmann, M.; Schiperski, F.; Zirlewagen, J.; Licha, T.  
655 Occurrence and Fate of the Angiotensin II Receptor Antagonist Transformation Product Valsartan  
656 Acid in the Water Cycle - A Comparative Study with Selected  $\beta$ -Blockers and the Persistent  
657 Anthropogenic Wastewater Indicators Carbamazepine and Acesulfame. *Water Res.* **2013**, *47* (17),  
658 6650–6659. <https://doi.org/10.1016/j.watres.2013.08.034>.
- 659 (56) Bertelkamp, C.; Reungoat, J.; Cornelissen, E. R.; Singhal, N.; Reynisson, J.; Cabo, A. J.; van der  
660 Hoek, J. P.; Verliefde, A. R. D. Sorption and Biodegradation of Organic Micropollutants during  
661 River Bank Filtration: A Laboratory Column Study. *Water Res.* **2014**, *52*, 231–241.  
662 <https://doi.org/10.1016/j.watres.2013.10.068>.
- 663 (57) Wiese, B.; Massmann, G.; Jekel, M.; Heberer, T.; Dünnebier, U.; Orlikowski, D.; Grützmacher, G.  
664 Removal Kinetics of Organic Compounds and Sum Parameters under Field Conditions for  
665 Managed Aquifer Recharge. *Water Res.* **2011**, *45* (16), 4939–4950.  
666 <https://doi.org/10.1016/j.watres.2011.06.040>.
- 667 (58) Hellauer, K.; Mergel, D.; Ruhl, A. S.; Filter, J.; Hübner, U.; Jekel, M.; Drewes, J. E. Advancing  
668 Sequential Managed Aquifer Recharge Technology (SMART) Using Different Intermediate  
669 Oxidation Processes. *Water* **2017**, *9* (221), 1–14. <https://doi.org/10.3390/w9030221>.
- 670 (59) Redeker, M.; Wick, A.; Meermann, B.; Ternes, T. A. Removal of the Iodinated X-Ray Contrast

- 671 Medium Diatrizoate by Anaerobic Transformation. *Environ. Sci. Technol.* **2014**, *48* (17), 10145–  
672 10154. <https://doi.org/10.1021/es5014714>.
- 673 (60) Su, T.; Deng, H.; Benskin, J. P.; Radke, M. Biodegradation of Sulfamethoxazole Photo-  
674 Transformation Products in a Water/Sediment Test. *Chemosphere* **2016**, *148*, 518–525.  
675 <https://doi.org/10.1016/j.chemosphere.2016.01.049>.
- 676 (61) Zuehlke, S.; Duennbier, U.; Heberer, T. Investigation of the Behavior and Metabolism of  
677 Pharmaceutical Residues during Purification of Contaminated Ground Water Used for Drinking  
678 Water Supply. *Chemosphere* **2007**, *69* (11), 1673–1680.  
679 <https://doi.org/10.1016/j.chemosphere.2007.06.020>.
- 680 (62) Massmann, G.; Dünnbier, U.; Heberer, T.; Taute, T. Behaviour and Redox Sensitivity of  
681 Pharmaceutical Residues during Bank Filtration - Investigation of Residues of Phenazone-Type  
682 Analgesics. *Chemosphere* **2008**, *71* (8), 1476–1485.  
683 <https://doi.org/10.1016/j.chemosphere.2007.12.017>.
- 684 (63) Briones, R. M.; Sarmah, A. K. Insight into the Sorption Mechanism of Metformin and Its  
685 Transformation Product Guanylurea in Pastoral Soils and Model Sorbents. *Sci. Total Environ.*  
686 **2018**, *645*, 1323–1333. <https://doi.org/10.1016/j.scitotenv.2018.07.251>.
- 687 (64) Torresi, E.; Polesel, F.; Bester, K.; Christensson, M.; Smets, B. F.; Trapp, S.; Andersen, H. R.;  
688 Plósz, B. G. Diffusion and Sorption of Organic Micropollutants in Biofilms with Varying  
689 Thicknesses. *Water Res.* **2017**, *123*, 388–400. <https://doi.org/10.1016/j.watres.2017.06.027>.
- 690 (65) Ramil, M.; El Aref, T.; Fink, G.; Scheurer, M.; Ternes, T. A. Fate of Beta Blockers in Aquatic-  
691 Sediment Systems: Sorption and Biotransformation. *Environ. Sci. Technol.* **2010**, *44* (3), 962–970.  
692 <https://doi.org/10.1021/es9027452>.
- 693 (66) Tülp, H. C.; Fenner, K.; Schwarzenbach, R. P.; Goss, K. U. PH-Dependent Sorption of Acidic  
694 Organic Chemicals to Soil Organic Matter. *Environ. Sci. Technol.* **2009**, *43* (24), 9189–9195.  
695 <https://doi.org/10.1021/es902272j>.

- 696 (67) Hoppe-Jones, C.; Dickenson, E. R. V.; Drewes, J. E. The Role of Microbial Adaptation and  
697 Biodegradable Dissolved Organic Carbon on the Attenuation of Trace Organic Chemicals during  
698 Groundwater Recharge. *Sci. Total Environ.* **2012**, *437*, 137–144.  
699 <https://doi.org/10.1016/j.scitotenv.2012.08.009>.
- 700 (68) Herzog, S. P.; Higgins, C. P.; McCray, J. E. Engineered Streambeds for Induced Hyporheic Flow:  
701 Enhanced Removal of Nutrients, Pathogens, and Metals from Urban Streams. *J. Environ. Eng.*  
702 **2016**, *142* (1), 04015053. [https://doi.org/10.1061/\(ASCE\)EE.1943-7870.0001012](https://doi.org/10.1061/(ASCE)EE.1943-7870.0001012).
- 703 (69) Herzog, S. P.; Higgins, C. P.; Singha, K.; McCray, J. E. Performance of Engineered Streambeds  
704 for Inducing Hyporheic Transient Storage and Attenuation of Resazurin. *Environ. Sci. Technol.*  
705 **2018**, *52* (18), 10627–10636. <https://doi.org/10.1021/acs.est.8b01145>.
- 706 (70) Peter, K. T.; Herzog, S.; Tian, Z.; Wu, C.; McCray, J. E.; Lynch, K.; Kolodziej, E. P. Evaluating  
707 Emerging Organic Contaminant Removal in an Engineered Hyporheic Zone Using High  
708 Resolution Mass Spectrometry. *Water Res.* **2019**, *150*, 140–152.  
709 <https://doi.org/10.1016/j.watres.2018.11.050>.
- 710 (71) Blaen, P. J.; Kurz, M. J.; Drummond, J. D.; Knapp, J. L. A.; Mendoza-Lera, C.; Schmadel, N. M.;  
711 Klaar, M. J.; Jäger, A.; Folegot, S.; Lee-Cullin, J.; Ward, A. S.; Zarnetske, J. P.; Datry, T.; Milner,  
712 A. M.; Lewandowski, J.; Hannah, D. M.; Krause, S. Woody Debris Is Related to Reach-Scale  
713 Hotspots of Lowland Stream Ecosystem Respiration under Baseflow Conditions. *Ecohydrology*  
714 **2018**, *11* (5), 1–9. <https://doi.org/10.1002/eco.1952>.
- 715  
716  
717  
718

719 **Supporting Information**

720 (1) Additional information on VFLUX 2.0 calculations and (2) TrOC analysis (Tables SI-01 & 02); (3)  
721 Description of the reactive transport model, DREAM settings, and molecular diffusion coefficients of  
722 TrOCs (Table SI-03); (4) Comparison of table reference compounds (Figure SI-01); (5) Median  
723 concentrations of TrOCs,  $\text{NO}_3^-$ -N, dissolved manganese and total dissolved iron in the surface water and  
724 in hyporheic porewater; (6) Measured hyporheic temperatures (Figure SI-02) and further discussion on  
725 DOC and  $\text{NO}_3^-$ -N dynamics in the HZ (Figures SI-03 & 04); (7)  $\text{pK}_a$  and  $\text{LogK}_{ow}$  values of investigated  
726 TrOCs (Table SI-05); (8) Pearson Product Moment correlations between  $\text{logD}_{ow}$  and calculated retardation  
727 coefficients; (9) Concentration time series and associated model fits (Figures SI-05 - SI-32) of all  
728 investigated TrOCs.

729

730

731

732

733 **Acknowledgements**

734 This project has been conducted within the Research Training Group ‘Urban Water Interfaces (UWI)’  
735 (Project N6 “Retention of chemical compounds in hyporheic reactors of urban freshwater systems”, GRK  
736 2032/1), which is funded by the German Research Foundation (DFG). This project has also received  
737 funding from the European Union's Horizon 2020 research and innovation programme under grant  
738 agreement No. 641939 (HypoTRAIN). We are grateful to three anonymous reviewers and the editor for  
739 discussion and comments on earlier versions of this manuscript.

740

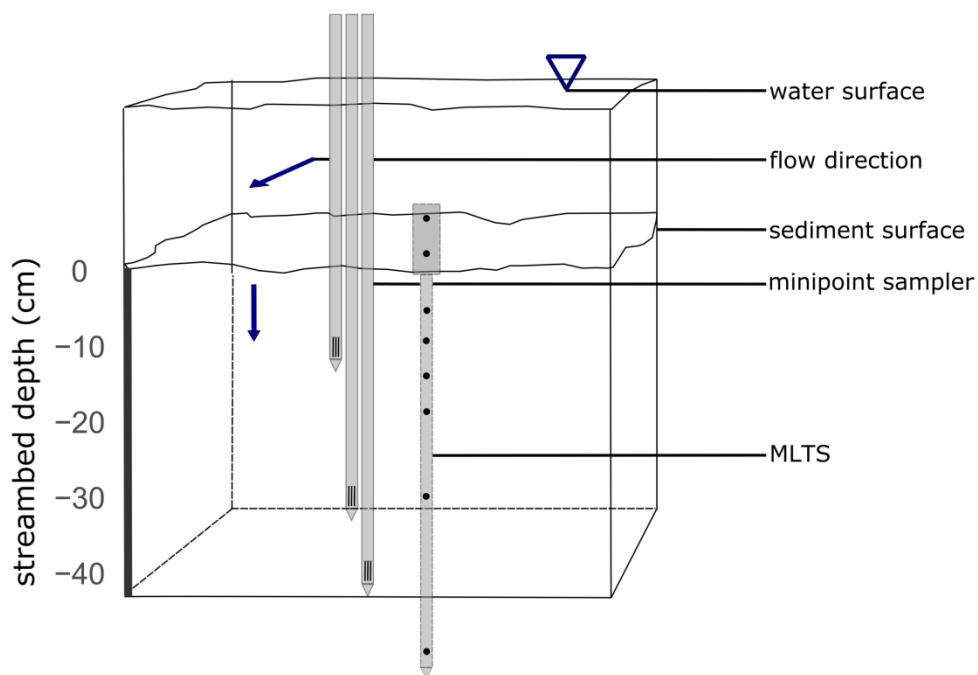
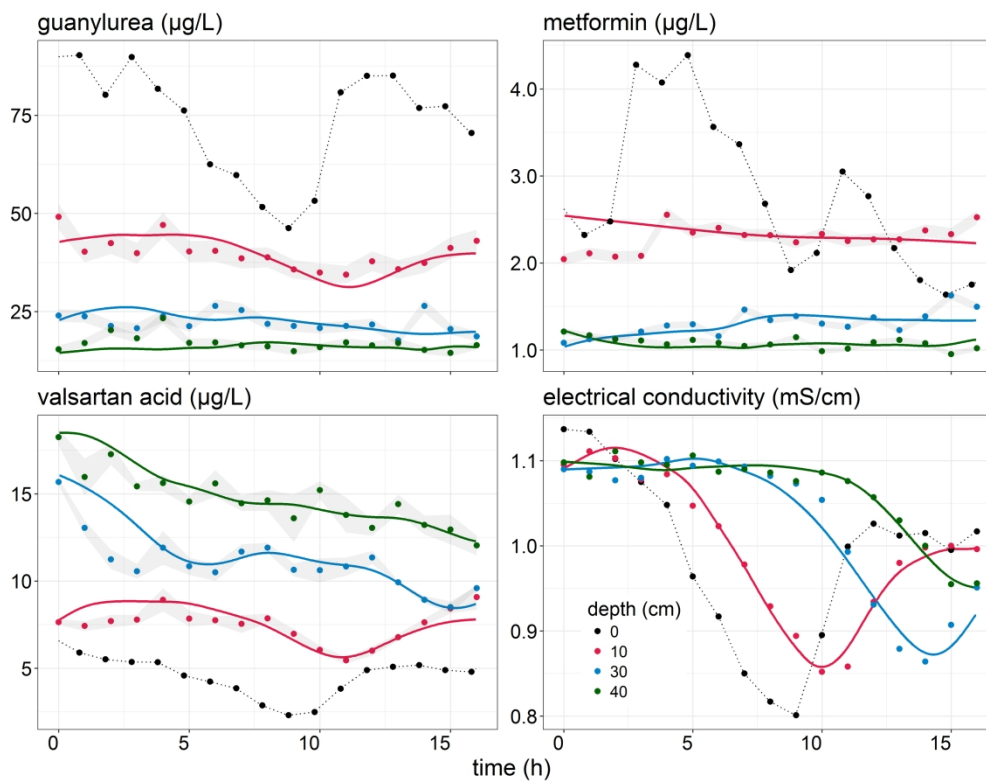


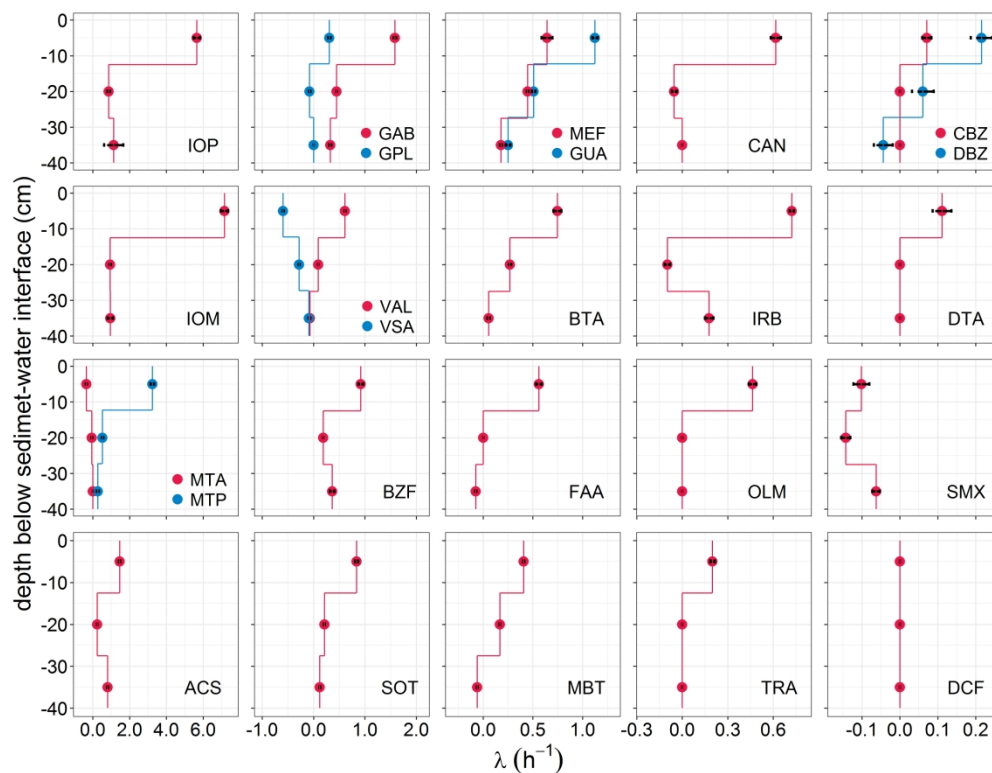
Figure 1 Experimental setup showing the three minipoint sampler installed in 10 cm, 30 cm and 40 cm depth in the hyporheic zone (HZ). The samplers were installed in a line ( $< 1$  cm distance) perpendicular to the water flow direction. A Multilevel Temperature Stick (MLTS) was installed in close proximity ( $\approx 10$  cm) next to the minipoint sampler array. Blue arrows indicate surface water and predominant hyporheic flow directions. Minipoint samplers were sampled from an aluminum bridge spanning the river channel (not shown).

200x139mm (300 x 300 DPI)



Measured (dots) and modeled (solid lines) concentration time series in 10 cm, 30 cm and 40 cm depth in the hyporheic zone (HZ) and measured concentration time series in the surface water (0 cm) of guanylurea (GUA), metformin (MEF), valsartan acid (VSA) and electrical conductivity (EC). For concentration time series measured in the HZ, analytical uncertainty (one standard deviation) is shown in grey. Note that for modeling purposes, concentration time series in the surface water were linearly interpolated (black dashed line) and that for EC no measurement uncertainties were available.

304x243mm (300 x 300 DPI)



First-order removal rate constants ( $\lambda$ ) as a function of depth of all investigated parent compounds (PCs, shown in red) and transformation compounds (TPs, shown in blue) except, primidone, epoxy-carbamazepine, venlafaxine and O-desmethylvenlafaxine. Error bars indicate one standard deviation. ACS, acesulfame; BTA, benzotriazole; BZF, bezafibrate; CAN, candesartan; CBZ, carbamazepine; DBZ, dihydroxy-carbamazepine; DCF, diclofenac; DTA, diatrizoic acid; FAA, 4-formylaminoantipyrine; GAB, gabapentin; GPL, gabapentin-lactam; GUA, guanylurea; IOM, iomeprol; IOP, iopromide; IRB, irbesartan; MBT, methylbenzotriazole; MEF, metformin; MTA, metoprolol acid; MTP, metoprolol; olmesartan, OLM; SMX, sulfamethoxazole; SOT, sotalol; TRA, tramadol; VAL, valsartan; VSA, valsartan acid.

304x243mm (300 x 300 DPI)